MICROCOPY RESOLUTION TEST CHART

ARO 13685.2-G

Engineering Experiment Station

LEVEL

EXPERIMENTAL MEASUREMENT TECHNIQUES

Final Report

Stuart A. Schleusener

August 1980

U. S. Army Research Office

Grant Number DAAG29-76-G-0165

Electrical & Computer Engineering
New Mexico State University
Las Cruces, New Mexico

EXPERIMENTAL MEASUREMENT TECHNIQUES

Final Report

Stuart A. Schleusener

August 1980

U. S. Army Research Office

Grant Number DAAG29-76-G-0165

Electrical & Computer Engineering
New Mexico State University
Las Cruces, New Mexico

(18) AKO (19) 13615.2-GEV

REPORT DOCUMENTATION PAGE	READ INSTRUCTIONS BEFORE COMPLETING FORM

1. REPORT NUMBER	2 GOVT ACCESSION NO.	3. RECIPIENT'S CATALOG NUMBER
	AD-A089 321	

4. TITLE (and Subtitle)	5. TYPE OF REPORT & PERIOD COVERED
EXPERIMENTAL MEASUREMENT TECHNIQUES	Final Report
	6. PERFORMING ORG. REPORT NUMBER

7. AUTHOR(s)	8. CONTRACT OR GRANT NUMBER(s)
Stuart A. Schleusener	DAAG29-76-G-0165

9. PERFORMING ORGANIZATION NAME AND ADDRESS	10. PROGRAM ELEMENT, PROJECT, TASK AREA & WORK UNIT NUMBERS
Electrical & Computer Engineering Box 3-O NMSU, Las Cruces, NM 88003	

11. CONTROLLING OFFICE NAME AND ADDRESS	12. REPORT DATE
U. S. Army Research Office P. O. Box 12211 Research Triangle Park, NC 27709	August 1980
	13. NUMBER OF PAGES

14. MONITORING AGENCY NAME & ADDRESS(If different from Controlling Office)	15. SECURITY CLASS. (of this report)
(12) 74	Unclassified
	15a. DECLASSIFICATION/DOWNGRADING SCHEDULE

16. DISTRIBUTION STATEMENT (of this Report)

Approved for public release; distribution unlimited.

17. DISTRIBUTION STATEMENT (of the abstract entered in Block 20, if different from Report)

18. SUPPLEMENTARY NOTES

The view, opinions, and/or findings contained in this report are those of the author(s) and should not be construed as an official Department of the Army position, policy, or decision, unless so designated by other documentation.

19. KEY WORDS (Continue on reverse side if necessary and identify by block number)

pellet spectrophone, spherical spectrophone, laser absorption, laser scattering

20. ABSTRACT (Continue on reverse side if necessary and identify by block number)

A pellet spectrophone has been designed and constructed to measure low level absorption by atmospheric dust and other particulate matter. It was shown that an absorption-to-scattering sensitivity greater than 50 can be achieved, which is a necessary property for measuring absorption at short wavelengths. Detection capability of microwatts of absorbed energy is also possible with this system. Therefore, milliwatt sources and microgram samples

DD FORM 1473 EDITION OF 1 NOV 65 IS OBSOLETE 389498 Unclassified

20.

may be utilized. Even though the pellet spectrophone responds primarily to absorbed energy it does not result in any data directly convertible to determination of the imaginary part of the complex refractive index except, perhaps under special conditions. This is due to problems regarding particle size distribution and involvement of the real part in scattering interactions. However, if all of these problems are recognized, use of the pellet spectrophone does result in good measurements of the absorption coefficients of the suspended material at whatever wavelengths tested and at whatever size distributions that exist in the host KBr pellet.

A resonant spherical spectrophone system was also designed and tested. This system proved to be very difficult to use because of its high Q characteristics. Small fluctuations in the resonance or chopper cause large signal variations. Although the system gain is high, the spectrophone is not as sensitive as expected. Wall and window effects amplified with the actual absorption signal reduce sensitivity.

TABLE OF CONTENTS

LIST OF TABLES

LIST OF FIGURES

INTRODUCTION

The use of electromagnetic laser energy by the Army for weapon guidance, surveillance, ranging, and remote sensing requires more information than is presently available concerning aerosol scattering and absorption of laser energy along propagation paths through the atmosphere. Measurements of aerosol extinction and in particular the aerosol absorption portion have lagged in recent years due to the difficulties of developing suitable laboratory measurement systems. Measurements of aerosol absorption and scattering in the open atmosphere are also desirable but have not easily been accomplished because of the long optical paths required and the lack of control of the environment. The work reported on herein concerns both a new laboratory absorption measurement system that has been developed and a resonant spherical spectrophone for either laboratory or insitu testing.

MEASUREMENT TECHNIQUES

PELLET SPECTROPHONE

The absorption of electromagnetic radiation by particulate matter
suspended in the earth's atmosphere is a quantity of considerable current
interest. However, most present day tests are being conducted in varying
forms of simulated laboratory environments due to the difficulty of open
atmospheric measurements. The pellet spectrophone is one of these forms
[1] and a system has been designed, constructed, and delivered.

The fundamental problem in making laboratory measurements of the ab-
sorption coefficient of atmospheric dust is in designing a technique
whereby the scattered energy and absorbed energy can be separately and
quantitatively determined. Spectrophones can be designed to respond
primarily to absorbed energy, thereby enabling separation. It should
be immediately noted that while the separation of scattered and absorbed
energies does take place and is important in itself, this does not nec-
essarily lead to determination of quantitative values of the imaginary
part of the complex refractive index. Also, the size distribution of the
suspended sample particles within the host pellet is in general unknown;
although, if needed, more effort can result in some distribution infor-
mation. However, even this may not be a handicap for cases where the
wavelength is known to be substantially greater than most particle
diameters. This occurs for the far infrared and submillimeter wavelength
regions.

The following is a list of some general techniques used for measuring
absorption characteristics. The first method, laser calorimetry [2],
measures the slope of the temperature versus time curve for a material
irradiated with laser energy of a specific wavelength. The second,
spectrophotometry [3], involves measurement of the transmission loss
through a sample. For the third technique, the emissivity of the sample
is measured at a specific temperature and then related to the absorption
coefficient [4]. Another technique is to gather light diffusely scattered
from a material and relate this to its scattering and absorption charac-
teristics [5]. For all of these methods, some problems are encountered.
This is because most of these techniques rely on some theory to relate
an observable parameter to the absorption, instead of measuring absorption

directly. Another major consideration is encountered at shorter wave-
lengths (visible and below). There, the particles are not small compared
to the wavelengths and scattering can become the dominant mechanism.

For the method described herein, energy absorbed heats the sample
which in turn heats an adjacent nonabsorbing gas. The resultant pressure
rise in the gas can then be interpreted as a direct measurement of the
amount of absorbed energy. This technique is known as photoacoustic
spectroscopy and provides potential applications in measuring spectral
characteristics of many materials [6,7]. This phenomenon, wherein a
constant-volume gas experiences a pressure increase due to radiation
absorption, was first observed by Alexander Graham Bell [8] in 1880.
Recognizing that this device could be used for measuring absorption
spectra, he gave it the name "spectrophone".

The spectrophone technique is especially useful in the measurement of
atmospheric dust absorption. In the past, a major problem has been to
separate effects due to absorption from those of scattering, especially
at shorter wavelengths. Spectrophones can be designed to respond pri-
marily to only that energy which is absorbed in the sample, since scattered
energy does not give rise to a temperature increase. This enables sepa-
ration of the absorption and scattering effects.

In order to relate this pressure signal to the absorption coefficient
of the material, the quantity of material must be known. For atmospheric
particulates, this aspect is overcome by mixing dust with KBr powder and_
pressing the dilute mixture with a steel die into a nearly clear disk.
The desired ratio of KBr to dust is obtained through the use of a high
accuracy analytic balance. Therefore, the sample pellet consists of the
atmospheric particulates suspended in a clear KBr host.

In view of the attributes in utilizing photoacoustic spectroscopy
for measuring low level absorption of laser energy by atmospheric dust,
a spectrophone system was developed to demonstrate several things. First,
it will be shown that a cell can be constructed which has minimal wave-
length dependence. Therefore, the spectrophone should be able to provide
quantitative absorption data on atmospheric dust from the visible to the
far infrared wavelength region. Secondly, it will be demonstrated that
a spectrophone system system can be selectively sensitive to the absorbed

energy in dust rather than scattered energy. Furthermore, several methods
for calibrating the spectrophone will be presented and compared. Finally,
preliminary measurement data on atmospheric dust for CO_2 laser wavelengths
and various other laser sources will be presented.

SPHERICAL SPECTROPHONE

In an attempt to investigate new structures and methods for measuring aerosol losses insitu, gaseous absorption tests were attempted in sphercally resonant structures.

A gas filled optoacoustic detector (spectrophone) is a device that measures attenuation by the media between the source and detector of those wavelengths absorbed by the sample gas. The system thus performs a measurement of the absorption coefficient of the gas sample.

Use of this concept was first proposed by Alexander Graham Bell [8] in 1880 when he observed that audible sound can be produced by exposing a gas in a transparent, constant-volume container to intensity-modulated infrared radiation. Since then, more refined methods have been introduced by Kruezer [9], Dewey, Kamm and Hackutt [10], and Rosengren [11]. All of these modern systems consist of a cylindrical spectrophone using a phase-sensitive lock-in amplifier for detecting the pressure waves created in the spectrophone. The cylinder usually has two apertures, one for the laser beam entrance and the other for the exiting beam. These apertures are normally arranged such that the beam passes lengthwise through the cylinder. The apertures are sealed with windows transparent to the laser used.

As the beam passes through the cylinder, it excites the molecules of the test gas to a higher state. When the beam is modulated, the excitation and relaxation of the gas molecules are detected by a micro- phone placed on the inside wall of the cylinder. This signal is then introduced to a phase-sensitive lock-in amplifier using the modulator signal as the reference source. The lock-in amplifier then extracts the true signal from the cylinder. The signal may have been buried in noise.

In hopes of increasing the sensitivity of spectrophones, a spherical geometry was investigated. In addition to the new geometry, it was operated at resonance. To further increase the signal detected by the spectrophone, the sphere was built with only one aperture to dump all the modulated laser energy into the sphere. It was hoped that the energy reflected off the walls would increase the activity of the test gas and therefore increase the signal out of the spectrophone.

Detection of the spectrophone signal using a phase-sensitive lock-in amplifier was virtually impossible due to the instability of the resonant signal. The phase setting on the lock-in amplifier had to be continuously adjusted since the phase relationship between the reference and the spectrophone signal changed as the sphere passed through resonance.

The instability of the detector signal prompted the use of a micro-computer for acquiring the data very rapidly. The data was then processed using a decimation-in-time FFT algorithm and converted to the frequency domain for interpretation.

CELL DESIGN CONSIDERATIONS

Figure 1 illustrates the basic configuration for the spectrophone cell. The fundamental assumption in using this cell for measuring absorption by atmospheric particulates (and other substances) is that the absorption coefficient is proportional to the pressure increase of the gas. A complete theoretical analysis has been given by H. S. Bennett and R. A. Forman [12,13,14]. Therefore, only their end results will be discussed here.

The basic cell consists of a nonabsorbing gas confined by two end windows and a cylindrical cell wall. At the center of the volume is the sample pellet mounted in a thermally insulating nylon holder. A laser beam propagates through the cell raising the temperature of the sample through absorption. The resulting increase in pressure of the gas is monitored by a capacitance manometer pressure sensor. The beam is not chopped, but is allowed to illuminate the sample for a relatively long time period so that a steady-state condition is reached. Bennet and Forman's theoretical analysis for several configurations show that the absorption coefficient should indeed be proportional to the pressure increase of the gas. Experimental verification using controlled dust suspensions in KBr pellets has also been observed in the laboratory.
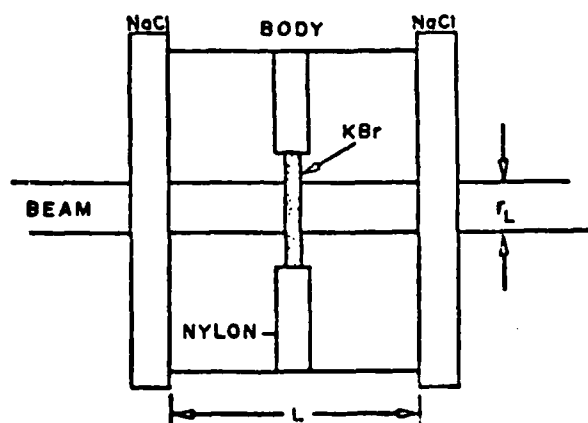

Figure 1. Basic Spectrophone Cell

Of course, all theoretical work implies that the sample thickness (or concentration) should be large for maximum signal. On the other hand, it can be shown that increasing the sample thickness (or concentration) also increases the time to reach steady-state conditions, thereby increasing the time for each pressure measurement. Actually, the turnaround time between measurements on different samples is primarily determined by removal and replacement procedures for the pellets. However, it is still important to hold down the illumination time period to reduce interference from other possible time varying changes.

Theory also predicts an increased sensitivity caused by decreasing the gas volume. This too has its limitations because of the desirability of allowing any scattered energy to exit the cell without striking the walls. Absorption in or at the wall surfaces can give rise to small erroneous signal components.

The power absorbed remains constant with respect to changing beam diameter. The source of heat might be envisioned as a percentage of the incident power absorbed over a specified cross-sectional beam area and depth of the sample. If the beam diameter is increased, the beam power is distributed over a larger area with a decreased power per particle. However, the beam encounters more absorbing centers. Therefore, the heat source appears constant under varying beam diameters. Also, a larger beam tends to average over any localized absorbing inhomogeneities in the sample.

Certain design criteria were set forth in an endeavor to obtain the optimum device. The following is a list of some of the major features that a good absorption measurement system should possess:

1. Ability to measure absorption directly
2. Minimal response to scattered energy
3. No system wavelength dependence
4. Mechanical and thermal stability

Along with these standards, an attempt was made to keep the system simple and relatively easy to operate. Utilizing the stated design criteria in conjunction with the existing theoretical framework; a spectrophone system was designed, developed, and tested.

GENERAL CELL DESCRIPTION

The ability of the spectrophone to measure absorption directly has been illustrated by theory and early experimental testing. Both show that measured pressure increases are proportional to the amount of energy absorbed in the sample. Therefore, the first criterion is met by using a spectrophone system. Due to the low absorption coefficients for most of the atmospheric particulates of interest, the small absorption in cell windows and the KBr of the sample pellet could override any pressure signal from the sample alone. Hence, a differential system [15] was adopted which effectively cancels the absorption signal from the windows and dust suspension material (KBr). Figure 2 illustrates the geometry of such a system.
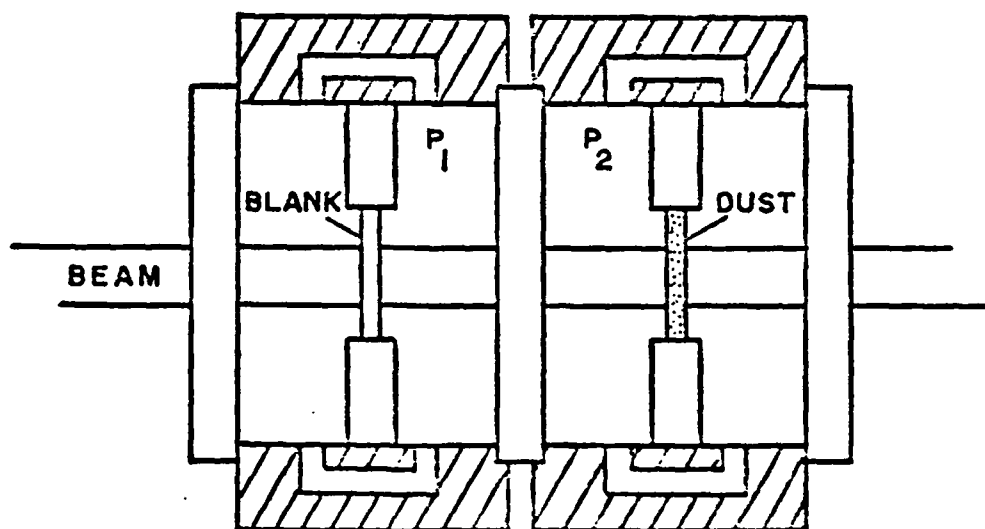

Figure 2. Differential Spectrophone Cell

A pressure sensor (capacitance manometer) is connected between the halves of the cell and it outputs a signal corresponding to the difference of the two pressures. Thereby, it is seen that if the materials are largely transparent to the energy, the signals from the windows should cancel. Also, the dust suspension material's effect is cancelled by placing a blank pellet in the opposite side of the differential spectrophone, leaving the signal due to the sample alone. This configuration allows measurement of very low absorption (microwatts).

Since the pressure signal from the sample alone is desired, as much of the scattered energy as possible must be allowed to exit the cell without being absorbed in the walls. This is accomplished by making the cell walls, and accordingly the windows, larger than the beam diameter, and having highly polished walls of large thermal mass to "sink" any heat which is not reflected. Consequently, constructing the spectrophone with substantial mass also enhances its mechanical stability while making it more insensitive to outside thermal influences. Because pressure sensitivity is dependent on the gas volume, instead of enlarging the cell inside diameter to allow the escape of scattered energy, the beam diameter is reduced through the use of a telescope.

The situation where energy is reflected by the different interfaces through the cell causes several problems. First any imbalance between that energy incident on either side of the differential spectrophone will cause an offset pressure signal. The offset must be reduced to a minimum so that the pressure sensor range may be adjusted for maximum sensitivity to the small signal of the sample.

Since a normal reflection loss per surface is approximately 4%, it is obvious that an offset will occur if no steps are taken to lessen this effect. Two methods are commonly used to minimize reflections. Either the interfaces must be tilted to the Brewster angle, or antireflection (AR) coatings must be applied. Tilting the windows reduces the usable cell aperture, thus increasing the likelihood of scattered energy striking the walls. Hence, the AR coatings were adopted.

Another problem encountered due to surface reflections occurs when they constructively and destructively interfere with each other to create a wavelength dependence in the spectrophone. This is another reason for AR coatings on all but the KBr pellets. Analysis of resonances in the KBr pellet is given in the following section.

-10-

WAVELENGTH RESONANCES

For the purpose of studying wavelength resonances in the spectro-
phone, it may be described as a stack of parallel-sided dielectric slabs
of varying thicknesses. Strictly speaking, a dielectric has zero absorp-
tion; while in practice the window and pellet materials do absorb to a
slight degree, the real part of the refractive index is by far the
determining factor for resonances in this case. Therefore, the materials
are assumed to be "true" dielectrics.

Constructive and destructive interference effects caused by multiple
reflections from the various boundaries in the spectrophone depend upon
the thickness relative to the wavelength of the incident illumination
and on the refractive indices of the constituent slabs. These interfer-
ence effects are described in terms of the complex transmission coeffi-
cients. From these coefficients the total transmission (denoted by T) of
the spectrophone may be obtained. To this end, a computer analysis program
was written to compute and plot the transmission of a stack of nondisper-
sive slabs over a specified wavelength range.

The object of this discussion is to outline the basic foundation of
the general theory [16,17] encountered in the analysis and describe the
computational methods involved.

Theory of Dielectric Layers

The instantaneous power flow per unit area (Poynting vector) may be
expressed by the equation

$$\vec{S} = \vec{E} \times \vec{H} \tag{1}$$

where

$$\vec{E}(\vec{r},t) = \text{Re } [\vec{E}_0(\vec{r})e^{i\omega t}] \tag{2}$$

and

$$\vec{H}(\vec{r},t) = \text{Re } [\vec{H}_0(\vec{r})e^{i\omega t}] \tag{3}$$

are the electric and magnetic field intensities, $\vec{r}$ the position vector
and $\vec{E}_0$ along with $\vec{H}_0$ the complex amplitudes of the vectors $\vec{E}$ and $\vec{H}$. The
symbol Re [ ] stands for "real part of".

For a plane wave propagating through a dielectric medium in the X direction,

$$\vec{S} = S_x \hat{X}$$

(4)

$\hat{x}$ being the unit vector in the direction of propagation and

$$S_x = (\frac{\varepsilon}{\mu})^{1/2} E_0^2 \sin^2 (\omega t - \beta x)$$

(5)

Since most laboratory instruments respond only to time-averaged values at optical frequencies, the average power must be used. To find the time-averaged power per unit area ($<\vec{S}>$), the instantaneous value given by (5) is integrated over one period and divided by the length of that period, giving

$$<S_x> = 1/2 (\frac{\varepsilon}{\mu})^{1/2} E_0^2$$

(6)

or

$$<\vec{S}> = 1/2 \eta E_0^2 \hat{x}$$

(7)

since the refractive index η is given by

$$\eta = (\varepsilon \mu)^{1/2}$$

(8)

with $\mu = 1$ for dielectrics.

The total transmission may be defined by the expression

$$T = \frac{\text{transmitted energy per unit area}}{\text{incident energy per unit area}}$$

where the "unit area" is parallel to the interface.
Thus,

$$T = \frac{<\vec{S}>_t \cdot \hat{n}}{<\vec{S}>_i \cdot \hat{n}}$$

(9)

where $\hat{n}$ is the unit vector in the direction normal to the boundary , and the suffixes i and t refer to the incident and transmitted beams.

Using vector algebra (9) can be rewritten as

$$T = \frac{\eta_t \, \text{Cos} \, \phi_t}{\eta_i \, \text{Cos} \, \phi_i} \left| \frac{E_t}{E_i}^2 \right|$$

(10)

ϕ_i and ϕ_t being the incident and refracted angles . Therefore, the transmission may be calculated if the incident and emergent mediums' refractive indices and electric magnitudes are known.

Matrix Approach

It is possible to obtain information about the incident medium's electric field by knowledge of the emergent medium's field. The expressions which relate the field components in adjacent media are obtained by using the boundary conditions of Maxwell's equations: i.e., that the tangential components of the electric and magnetic fields are continuous across a boundary between any two media. Weinstein [18] has described a convention of notation in which the field quantities in any slab consist of both a positive (incident) and negative (reflected) propagating wave. If this convention is adopted, the expressions for the tangential components of the electric and magnetic fields at the boundary between the 0 (incident) and 1 (emergent) media are

$$H_0^+ = U_0 E_0^+ \tag{11}$$

for the incident beam, and

$$H_0^- = - U_0 E_0^- \tag{12}$$

for the reflected beam, while

$$U_0 = \frac{\eta_0}{\cos\phi_0} \tag{13}$$

for a parallel polarized E-field, and

$$U_0 = \eta_0 \cos\phi_0 \tag{14}$$

for a perpendicular E-field.

The sums of the fields created by the two beams are

$$H_0^+ + H_0^- = H_1^+ e^{ig_1} + H_1^- e^{-ig_1} \tag{15}$$

and

$$E_0^+ + E_0^- = E_1^+ e^{ig_1} + E_1^- e^{-ig_1} \tag{16}$$

where g_1 represents the phase thickness between the (0,1) and (1,2) boundaries. Or, equivalently,

$$g_1 = \frac{2\pi}{\lambda} \eta_1 h_1 \cos \phi_1 \tag{17}$$

where

-13-

η_1 = refractive index of medium 1

h_1 = thickness of medium 1

ϕ_1 = angle of incident beam to surface normal.

Substituting (11) and (12) into (16) gives

$$U_0(E_0^+ - E_0^-) = U_1(E_1^+ + e^{ig_1} - E_1^- e^{-ig_1})$$ (18)

from (16) and (18), solving for $E_0^{\pm}$,

$$E_0^{\pm} = \frac{1}{2U_0} [(U_0 \pm U_1)e^{ig_1} E_1^+ + (U_0 \mp U_1)e^{-ig_1}E_1^-]$$ (19)

(and likewise for $H_0^{\pm}$).

Equation (19) relates information about the E-field in the incident medium from knowledge of that in the emergent medium.

Allowing the total electric and magnetic fields in the emergent medium to be given by

$$E_1 = E_1^+ + E_1^-$$ (20)

and

$$H_1 = H_1^+ + H_1^- = U_1(E_1^+ - E_1^-)$$ (21)

and substituting these yields (in matrix form)

$$\begin{pmatrix} E_0 \\ H_0 \end{pmatrix} = \begin{pmatrix} \cos g_1 & iU_1^{-1} \sin g_1 \\ iU_1 \sin g_1 & \cos g_1 \end{pmatrix} \begin{pmatrix} E_1 \\ H_1 \end{pmatrix}$$ (22)

i.e.,

$$\begin{pmatrix} E_j \\ H_j \end{pmatrix} = M_{j+1} \begin{pmatrix} E_{j+1} \\ H_{j+1} \end{pmatrix} = M_{j+1}M_{j+2} \begin{pmatrix} E_{j+2} \\ H_{j+2} \end{pmatrix} = \text{etc.}$$ (23)

Thus, the "characteristic matrix" M for the total stack is equal to the product of the slab matrices.

From (10) the transmission is given as

$$T = \frac{U_N}{U_0} \left| \frac{E_N^+}{E_0^+} \right|^2$$

(24)

where 0 is the incident medium and N is the emergent medium. And, by definition, the transmission coefficient t is expressed as

$$t = \left(\frac{U_N}{U_0} \right)^{1/2} \left| \frac{E_N^+}{E_0} \right|$$

(25)

since

$$T = |t|^2$$

(26)

Therefore, from (25) and the characteristic matrix of the total stack, t is found to be

$$T = \left(\frac{U_N}{U_0} \right)^{1/2} \frac{2U_0}{M_{11}U_0 + M_{22}U_N + M_{12}U_N U_0 + M_{21}}$$

(27)

In general, the elements M_{ij} of the matrix M are all complex. Also, there are as many 2X2 characteristic matrices as there are slabs. Therefore, the main labor encountered in evaluating the total transmission is in performing the matrix multiplication, a chore well suited to digital computers.

Computational Method

An interactive computer program (see Appendix) was written to calculate and plot the total transmission of a series of dielectric slabs over a specified wavelength range based on the theory just presented. A simplified flowchart of this program is given in Figure 3. Data input consists basically of the following:

Beam polarization (S or P)

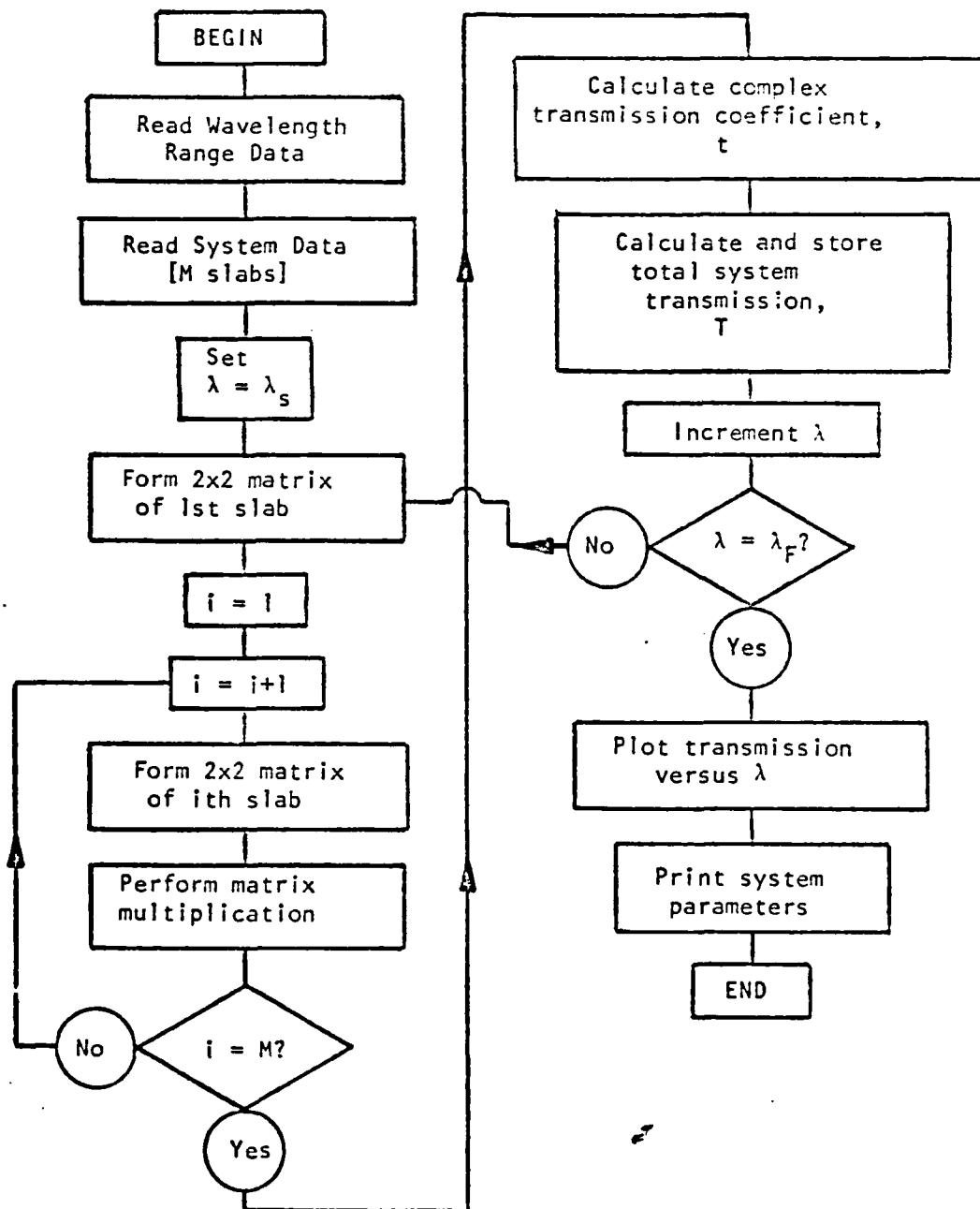m   Number of slabs and air gaps

η_0 Index of incident medium

Figure 3

Flowchart for Resonance Computer Program

$$\left.\begin{array}{c} \eta_1 \\ \\ \\ \\ \\ \eta_{N-1} \end{array}\right]$$
refractive index of each slab

η_N Index of emergent medium

λ_S Start wavelength

λ_F Finish wavelength

N   Number of steps

For each wavelength the characteristic matrix (22) of each layer is formed. Secondly, the m 2x2 matrices are multiplied together with the transmission coefficient calculated as in (27). Finally, the total transmission is computed according to (26) and stored in memory. This process continues for the specified wavelength range ending in the total transmission being plotted versus wavelength on a graphics terminal. Interactive options are available to the user for changing parameters, printing tables, etc

Computational Results

The purpose of this program was to qualitatively illustrate the magnitude of the problems encountered with wavelength resonances in the spectrophone. The initial differential spectrophone consisted of three _ NaCl polished windows, two pressed KBr pellets, and four air gaps (nine slabs total). A typical plot for the transmission of the KBr pellet within the Co_2 laser wavelength range is illustrated by Figure 4. Note that the period of resonance is 0.047 micrometer. Likewise, Figure 5 represents the transmission characteristics of the salt windows. Accordingly, the period of this plot is much smaller (0.005 micrometer), due to the increased thickness. Obviously, the effect of either the KBr pellet or NaCl window taken alone would not create too many problems, since at least 80% of the energy is passed for all wavelengths in this range. On the other hand, when the total system configuration is taken into account (Figure 6), severe problems arise. Here, transmission can drop to as low as 10% for certain wavelengths. This means that the spectrophone signal would vary considerably between certain wavelengths due to less energy reaching the sample pellet, instead of only responding to more or less absorption in the sample.
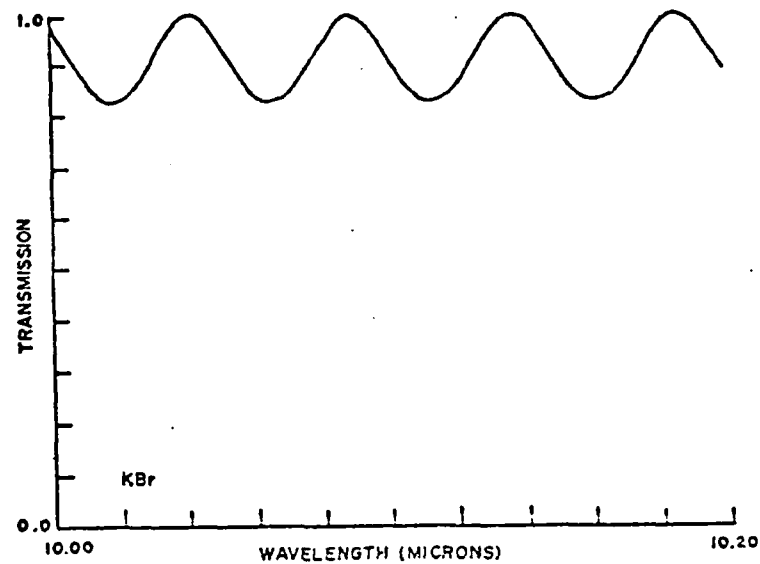
Figure 4

Computer Transmission Plot
for 0.686mm Thick KBr Pellet
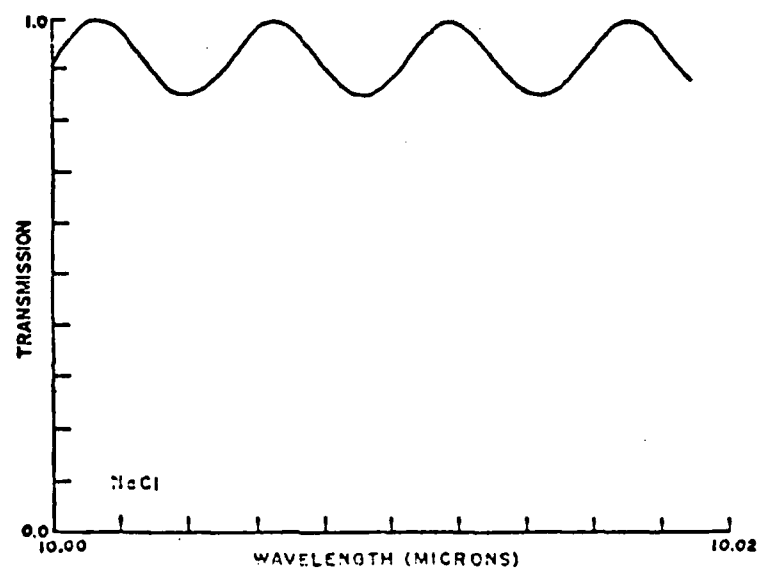
Figure 5

Computer Transmission Plot
for 6.35mm Thick NaCl Window
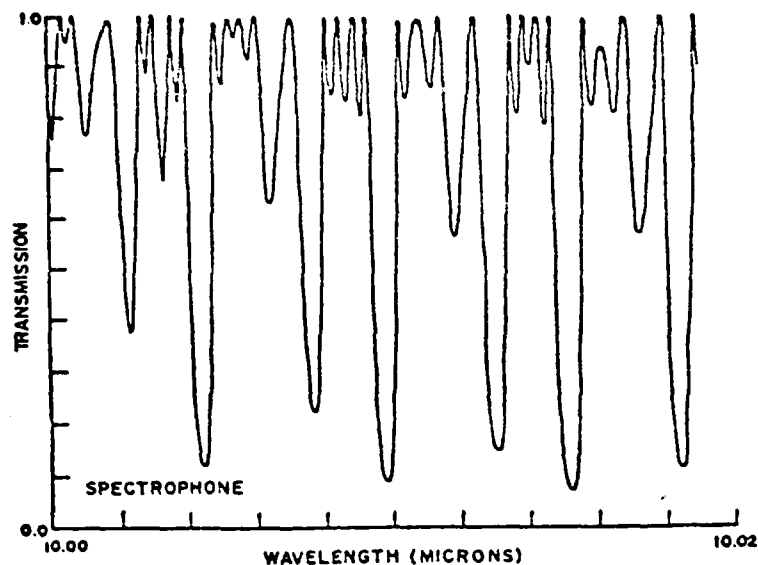
Figure 6

Computer Transmission Plot for Differential Spectrophone

Another problem encountered is multiple reflections through the sample; this increases the effective sample thickness. These multiple reflections might arise from surfaces on either side of the sample or internal to the sample pellet itself. Consequently, an erroneously large signal would result.

These resonance problems would be especially critical in regions of high absorption. In these regions small changes in the amount of energy available to the sample for absorption give rise to large variances in the pressure signal. On the contrary, for wavelength regions where the sample is relatively transparent to the laser energy, the same change would produce less signal variance due to smaller absorption.

From this discussion, it is seen that wavelength resonances in the

spectrophone can create severe problems when attempting to measure absorption characteristics. Furthermore, these effects are especially pertinent when using tunable lasers in obtaining absorption spectra. The next chapter discusses means of minimizing this phenomenon.

EXPERIMENTAL PROCESS AND RESULTS

This section discusses the total spectrophone system built to measure atmospheric dust absorption in a laboratory environment. The apparatus is described, test and calibration methods explained, and results of preliminary investigations presented.

Various laser sources were utilized to demonstrate the usefulness of the differential spectrophone over a wide wavelength range. Among these sources were the HeNe (0.63, 1.15, and 3.39 μm), Nd:YAG (1.06 μm), DF (3.8 μm), and tunable CO_2 (9.2 to 10.8 μm) lasers. As pointed out in previous sections, the absorption of CO_2 laser energy by atmospheric particulates is of special interest. Hence, the following description pertains to system use in CO_2 laser tests only. The system is basically the same for all sources, with obvious amendments to wavelength dependent components such as AR coatings, wavelength analyzers, etc.

Apparatus

Figure 7 is a block diagram of the system setup with beam routing as indicated. All components are rigidly mounted on a massive 3 by 6 foot steel optics table to minimize any mechanical vibrations or component shifting. The light source is a commercially available, water-cooled, tunable CO_2 laser. It operates at approximately 40 discrete wavelengths over a range from 9.2 to 10.8 micrometers. The output beam for an average line has vertical polarization, TEM_{oo} mode purity, 5 millimeter diameter at e^{-1} points, and a minimum continuous power of 3 watts. Tuning is accomplished by changing the tilt of the diffraction grating making up the back end of the laser cavity. Also, by changing the length of the cavity with a piezoelectric crystal attached to the grating, output power at the selected transition is maximized. Long-term frequency stability is better than 5 megahertz over several hours. Short-term (0.1 second) variations are less than 50 kilohertz.

Wavelength identification is accomplished by utilizing a CO_2 wavelength spectrum analyzer. This instrument is a grating spectroscope which has a calibrated uv excited thermal sensitive strip in the output plane. Diffracted infrared energy heats the strip at the calibrated
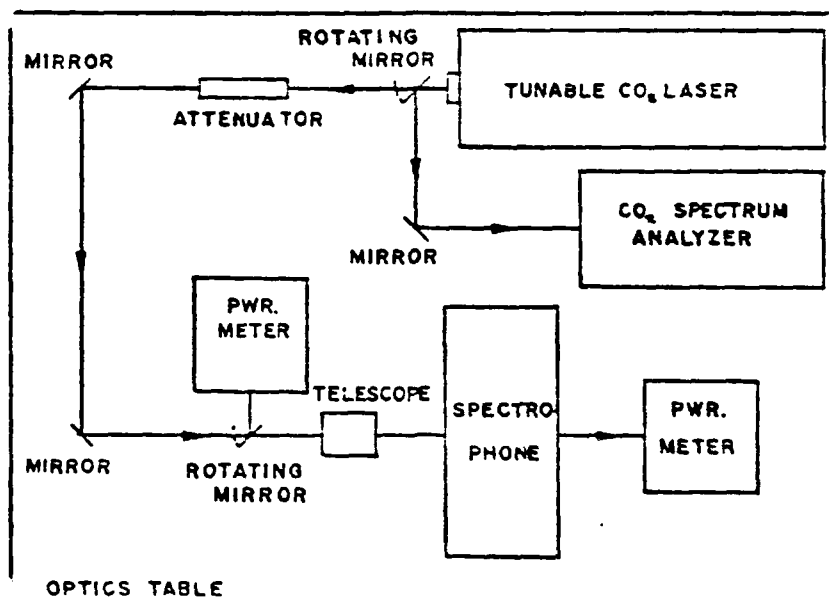
```
                    ROTATING
                     MIRROR
  MIRROR                        ┌─────────────────────┐
         ┌──────────────┐       │  TUNABLE CO₂ LASER  │
         │  ATTENUATOR  │       └─────────────────────┘
                                      ┌──────────────────┐
                                      │  CO₂ SPECTRUM    │
                                      │  ANALYZER        │
                     MIRROR           └──────────────────┘
         ┌──────────┐
         │  PWR.    │
         │  METER   │        ┌─────────┐  ┌──────┐
         └──────────┘ TELESCOPE│ SPECTRO │  │ PWR. │
                              │ PHONE   │  │ METER│
  MIRROR    ROTATING          └─────────┘  └──────┘
            MIRROR

  OPTICS TABLE
```

Figure 7. System set-up

wavelength position, causing it to darken. Beam mode structure observa-
tion and beam alignment is also accomplished by using uv excited flores-
cent beam probes.

Due to the high minimum energy developed by this CO_2 laser, a varia-
ble beam power attenuator is incorporated into the system. This is neces-
sary to prevent damage to the sample pellet through excessive heating.
It is also useful in obtaining a good signal-to-noise ratio for the
desired pressure sensor range and sample used. Beam attenuation is
accomplished by rotating two Brewster-angled flats around the beam axis.
Since the laser output is polarized vertically, 2% to approximately
95% attenuation occurs for respective rotation angles of 0^{0} and 90°.
Beam power is then monitored by two disc calorimeters.

As previously mentioned, a telescope is used to decrease the diameter
of the beam through the spectrophone cell. This is done for scattering

and time response considerations. The optical elements used in the telescope are two germanium f/1 lenses with focal lengths of 1.5 and 1.0 inches. Both lenses are AR coated for operation at the CO_2 laser wavelengths. By mounting the two lenses in a lens translation mount, the desired telescope focal length is attained.

Two adjustable aluminum front-surface mirrors at the end of the optics table are used to fold the optical path. This enables the height and horizontal translation of the beam to be adjusted so it will pass through the stationary spectrophone cell without striking the walls. Furthermore, the two rotatable aluminum mirrors are used to interrupt the beam and route it to the spectrum analyzer for wavelength identification and to the power meter for monitoring power prior to running a test. These mirrors are mounted on electric solenoids which are activated by remote switches.

Figure 8 illustrates the spectrophone platform layout. The components are bolted to an aluminum plate which elevates the spectrophone to a beam height of 7.5 inches. The platform is enclosed by a removable cover that insulates the components from stray illumination and heat. This is used since the spectrophone is constructed to be very sensitive to small pressure increases. The gas filling valve stems and leak valve adjusting micrometer are allowed to extend outside of the thermally insulating cover so that the spectrophone is not affected by body heat in adjusting the system. Also, insulating foam rubber surrounds all components except the spectrophone cell itself. All valves, tubing, and connectors are stainless steel. Furthermore, the tubing is thickwalled to minimize thermal effects and cell gas volume, the latter being necessary for increased pressure sensitivity.

Figure 9 is a full-scale drawing of the differential spectrophone. The antireflection coated zinc selenide windows were measured with a spectrophotometer to have a total attenuation per flat of approximately 0.5% over the CO_2 laser wavelength range. The body is machined of 4-inch diameter round aluminum stock and polished inside to a mirror-like finish. The cell is milled flat on the bottom so that it is in good thermal contact with the supporting plate. This acts as a thermal shunt between the two halves of the cell, thereby equalizing any thermal differential between
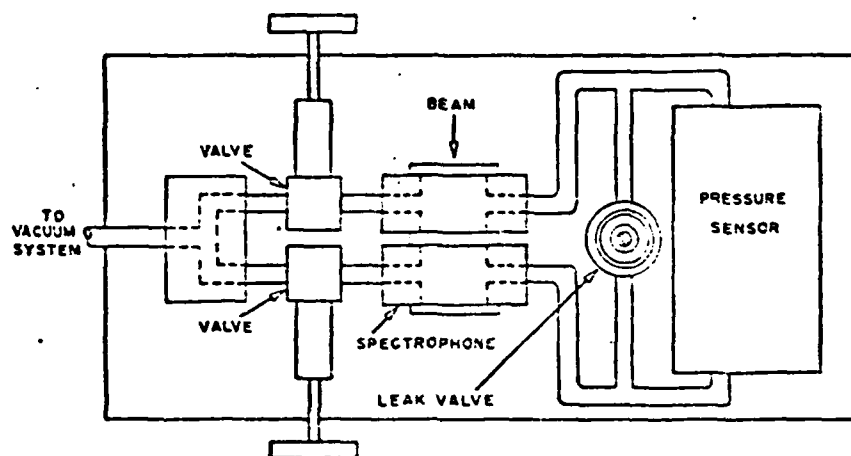
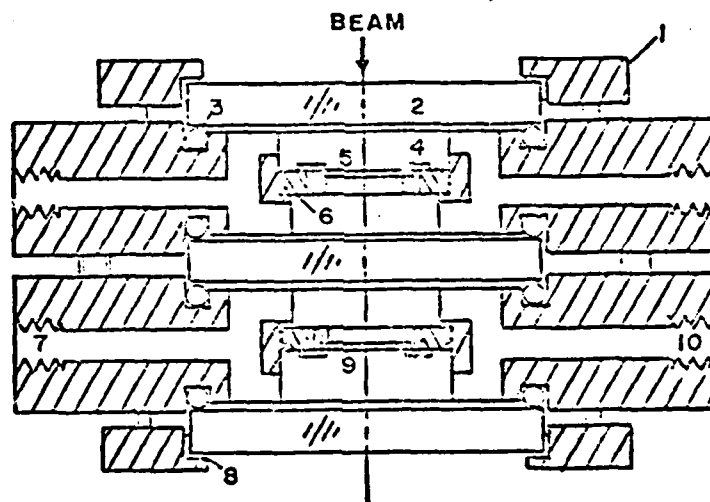Figure 8. Spectrophone platform

· Figure 9:

Differential Spectrophone

1. Window retaining ring

2. Antireflection coated ZnSe window

3. Neoprene O-ring

4. Nylon retaining screw

5. Blank KBr pellet

6. Nylon pellet holder

7. Gas-filling and evacuating port

8. Silicon sealant

9. Sample pellet

10. Pressure sensor port

them. It also increases the thermal mass used to "sink" away heat raised by scattered energy striking the walls. Care must be taken to assure that no solvent or oil is left on the body since outgassing can cause the foreign gas to absorb energy. The system was baked in a vacuum oven to remove all residue.

The pellets are made by pressing the powdered KBr mixture in a steel die. The optimum amount of material for a clear pellet, a reasonable signal, single scattering, and short time response was found to be 250 milligrams. This material is pressed with a pressure of 25,000 pounds per square inch under vacuum for several minutes. Possible internal wavelength resonances in the pellet are minimized by dimpling the surfaces of the die so that there are no parallel interfaces. The resulting disc is placed in a nylon holder and inserted into the spectrophone with a specially made spanner wrench.

The pressure sensing element is a commercially available capacitance manometer. A highly prestressed metal diaphragm is the variable element in a high precision capacitive potentiometer (Figure 10). The diaphragm is positioned between fixed capacitor plates and forms the separation of two gas tight enclosures connected to opposite sides of the differential spectrophone. A difference in total pressure across the partition causes it to deflect, thereby changing the capacitance of the diaphragm and fixed capacitor plates. This variable capacitor is part of a 10 kilohertz carrier excited bridge. The changing capacitance unbalances the bridge which in turn produces a 10 kilohertz output voltage having an amplitude proportional to the applied pressure difference. Hence, the output signal is directly related to the pressure of the gas.

This signal is then conditioned to a ±10 volt d.c. full-scale amplitude with a ±0.01% linearity. Range multiplier positions are available to change the pressure range for the sensor being used. In this case a 0 to 1 Torr sensing head is used with an ultimate resolution of 2×10^{-6} Torr. Up to 20 psi overpressure may be applied without damage because the diaphragm makes contact with a static capacitor plate which takes up the load.

The leak valve in Figure 8 is a precision gas metering valve. Metering is accomplished by a microgrooved pin being moved by a non-rotating bellows sealed micrometer actuator. Typical leak rates are illustrated in Figure 11. The leak valve is set (very nearly closed)

A SUBSTRATE SUPPORT
B SEALED HOUSING
C SCREEN
D JUMPER WIRE

E CERAMIC SUBSTRATE
F FILM TERMINATION
G GOLD FILM
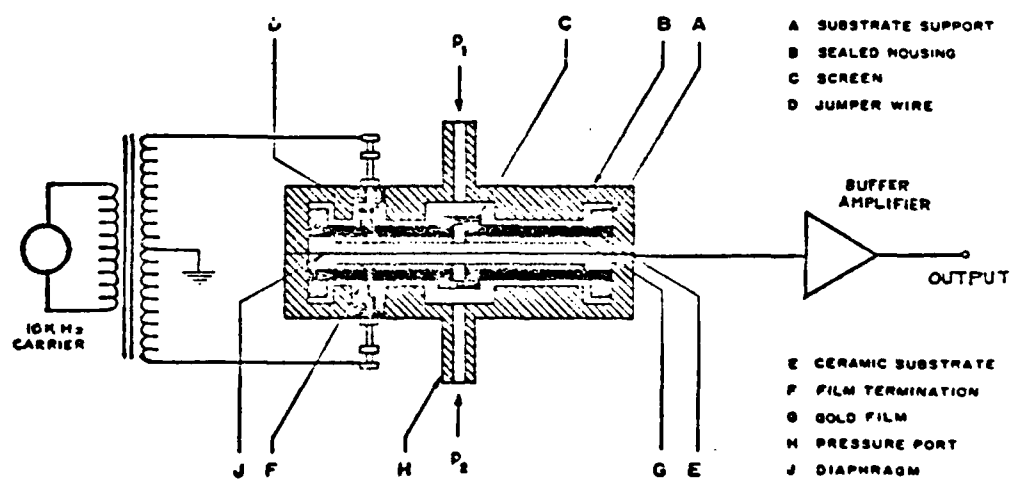H PRESSURE PORT
J DIAPHRAGM
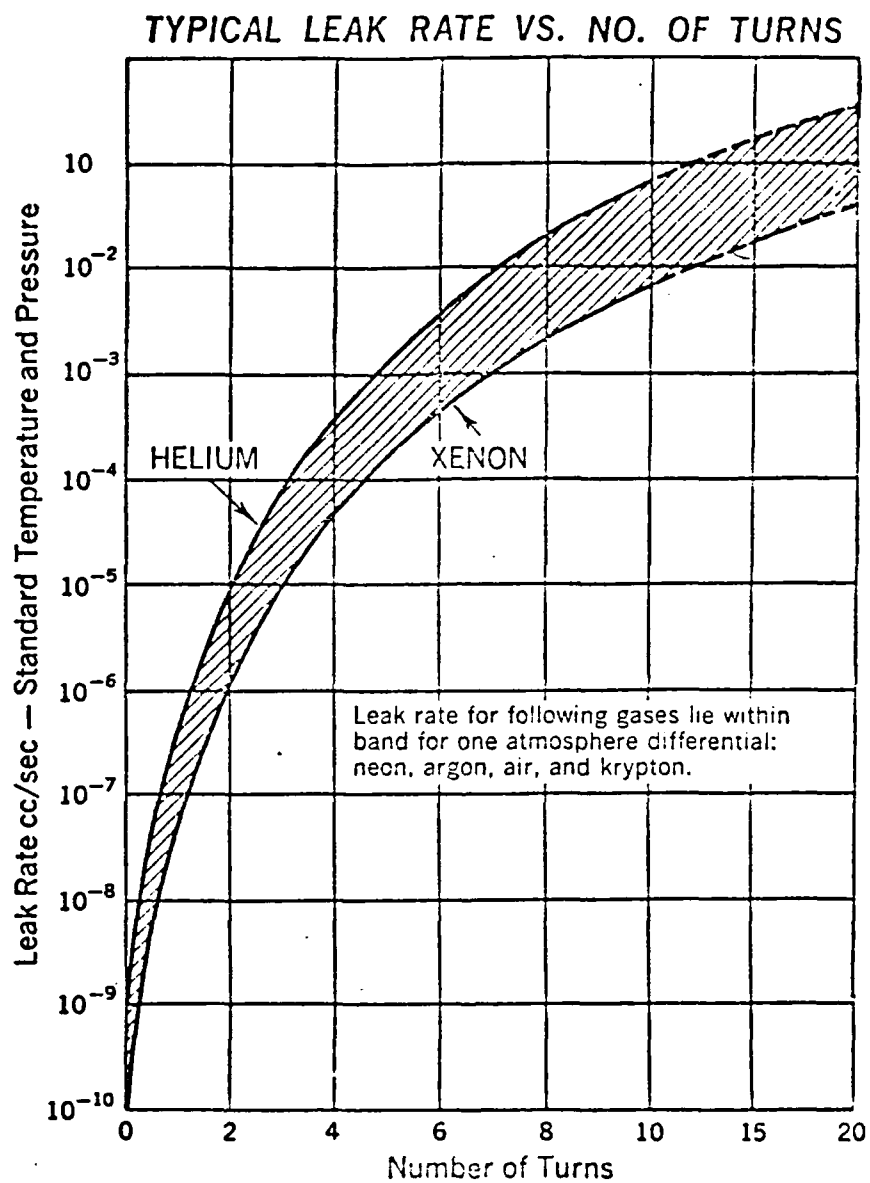
Figure 10. Capacitance manometer

Figure 11. Leak-valve setting

so that it nearly isolates the halves of the cell from each other during the test period and yet maintains steady-state pressure equilibrium. Thus, the pressure difference between the front and back sections of the spectrophone caused by small leaks, out-gassing, and likes is automatically equalized before a test is initiated. Once the leak valve is set, it should not be changed without recalibrating the system.

Test Procedure and Calibration

First, the offset signal present in the spectrophone must be measured. To do this, a 250 milligram blank KBr pellet is made to be placed in both the front and back chambers. Care must be taken not to touch or breathe on the KBr powder or resulting pellet since it is very hygroscopic. To prevent any water absorption, the KBr powder and powder/sample mixtures are kept in a vacuum oven until needed. The material is weighed by an analytic balance, agitated by a mechanical vibrator, and placed in the pellet die. These processes are all done on a clean bench to prevent any contamination by lab air dust. Next, the KBr is pressed into a pellet. The pellet is then weighed and the weight recorded. This process is repeated for all pellets made whether blank KBr or sample mixtures.

With a 250 milligram blank KBr pellet in both sides of the spectrophone, and assuming the leak valve is adjusted as in Figure 12 [1], the test is initiated. The cell is back-filled with 660 Torr (local atmospheric pressure) of nonabsorbing N_2 gas. The laser wavelength is adjusted by the grating micrometer while observing the spectrum analyzer and the power via the variable attenuator and power meter in front of the spectrophone. Secondly, after the cell has reached pressure equilibrium, the rotatable mirror in front of the cell is deactivated, thus allowing the beam to pass through. The resultant signal from the capacitance manometer is observed on a digital voltmeter until a peak is reached. This is the offset signal inherent to the system and is subtracted from or added to (depending on the direction of the offset) all sample signals. The cell output level is also recorded at this time.

For a sample test, the same process is repeated (except a dust pellet is in the back) with the addition of a pellet extinction test. Here the back ZnSe window is removed and the power level at the rear power meter
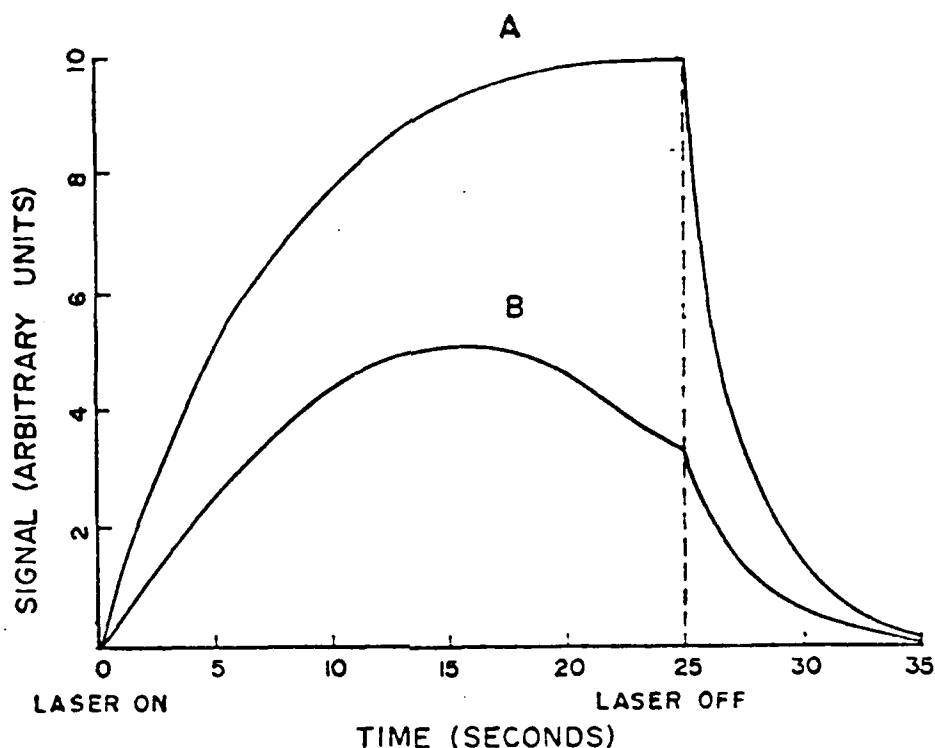
Figure 12. Spectrophone output signal. (A) Desired
leak-valve setting. (B) Leak-valve far open.

is recorded with both the sample pellet in and out of the beam. The
difference of these two signals corresponds to the power lost due to
reflection and absorption by the sample pellet.

Initial calibration tests were performed using three different ap-
proaches: CO_2 gas absorption; ir extinction measurements; and nichrome
wire dissipation. Test calibration results using the first two methods
agree within ±10% at this stage.

The CO_2 gas calibration procedure consists of using a CO_2 laser
source and a known CO_2 absorption line such as P(20) at 10.59 micrometers.
A CO_2-N_2 gas mixture is placed in the back chamber, while only N_2 is
inserted in the front chamber at the same total pressure. Pure KBr
pellets are in both the front and back chambers to keep both volume and
balance test conditions as similar as possible to those encountered when
making pellet particulate absorption tests. Between 150 Torr and 200
Torr of CO_2 is used due to the short path length in the particulate

spectrophone back chamber. The CO_2 laser source is tuned to the P(20) 10.59 micrometer line center and chopped at about 0.25 Hertz, as compared to the steady-state method used for particulate tests. This faster on-off rate is possible due to the shorter CO_2 gas absorption energy transfer rate. The 150 to 200 Torr CO_2 pressure makes it necessary to include self-broadening effects along with the N_2 foreign broadening. In addition, the comparative thermal properties of CO_2 and N_2 must be taken into consideration because of their great difference. A calibration absorption sensitivity figure of about 470 ±30 V/W absorbed was obtained for the 0.03 capacitance manometer scale and a leak valve setting resulting in a 20-second test period for a 250 milligram pellet.

A second approach to calibrating the differential spectrophone involves use of a highly absorbing sample pellet such as acetylene soot in the 10 micrometer wavelength region. Since scattering can be approximated as being negligible compared to soot absorption at these wavelengths, an extinction test can be compared to the spectrophone signal obtained by using the same pellet.

After pellet gas-to-solid boundary reflection losses of about 8% are subtracted, the remaining loss due mostly to absorption can be equated to the spectrophone signal. The resulting absorption sensitivity figure of 450±30 V/W compares well with the CO_2 derived figure of 470 V/W. Considering differences between the two methods, these numbers agree quite favorably.

The third approach to calibration uses a coil of nichrome wire placed in the back chamber. By measuring the resistance of the coil, a known amount of energy can be dissipated and the corresponding pressure change converted to a voltage signal by the capacitance manometer. During the calibration tests, it was discovered that the position of the coil in the back chamber is an important factor in the calibration results obtained. It was also determined that the time constant of the wire itself is substantially less than the pellet-chamber interaction. Part of these difficulties were overcome by having the nichrome wire would in a flat coil geometry and placed in the position of the back chamber pellet. The difficulty of minimizing heat leakage out of the chamber along the wire leads was never really overcome. Therefore, attempts at calibration using a coil of nichrome wire always were unsuccessful and,

in general, resulted in calibrations about one-half as large as the CO_2 gas and extinction pellet approaches.

Test Results

Lambert's law is used to calculate the absorption coefficient from the experimental data of the preliminary studies. Use of this law assumes single scattering and only one pass of the beam through the sample. These are simplifying assumptions which may not always hold, but they are satisfactory for these early tests. Particle size (with respect to wavelength) also appears to be an important factor when comparing absorption data from different methods because of the possible effect on absorption per unit mass of sample. This effect became apparent when discrepancies occurred between quartz data obtained from the spectrophone and those obtained by other methods [19]. Photomicrographs of the sample showed quartz particles much larger (25 μm) than the wavelengths of the CO_2 laser. Therefore, in order to compare different absorption data, the sample particulate size must be taken into account. This may become useful in future attempts to determine particulate size-absorption effects.

Lambert's law is given by

$$P = P_o \exp (-kx) \tag{28}$$

where x is the effective sample thickness in centimeters, P_o is the incident power, and k is the absorption coefficient.

The reflection loss at the incident pellet interface was measured to be 4% of the power, independent of the sample used, and constant over the wavelength range. The energy reflected back through the sample by the back pellet surface is also approximately 4% of the incident energy (due to the low absorption), but it gives rise to sample heating. Therefore, the effects of reflection at the incident and emerging surfaces of the pellet approximately cancel. Hence, for signal considerations, from conservation of energy,

$$P = P_0 - P_A \tag{29}$$

Where P_A is the power absorbed in the sample. Rewriting (28) by using (29) and solving for the absorption coefficient gives

$$\tag{30}$$

-31-

The power absorbed (P_A) is found by dividing the recorded manometer
signal by the system calibration sensitivity; or equivalently,

$$P_A = \frac{\text{manometer signal (V)}}{\text{sensitivity (V/W)}}$$

(31)

The incident power (P_o) was recorded with the pellet and back window
removed.

The next step is to find the effective sample thickness x. For
this calculation a particulate mass density (ρ) is assumed. The ratio
of sample dust to KBr is calculated by dividing the measured mass of the
sample used in the dilution process by the sum of the masses of the KBr
and sample. Multiplying this quantity by the weight of the pellet gives
the number of grams of sample per pellet; or

$$\text{ratio} \times 250 \text{ mg} = \frac{\text{sample weight}}{\text{pellet}}$$

(32)

By dividing (32) by the assumed sample density, the volume of the sample
per pellet is found. Assuming the dust is distributed uniformly through-
out the pellet, the effective sample thickness is obtained by dividing
the volume of sample per pellet by the pellet surface area; or

$$\frac{\text{sample volume}}{\text{pellet}} = \frac{\text{sample wt. per pellet}}{\text{sample density } (\rho)}$$

(33)

$$x = \left(\frac{\text{sample volume}}{\text{pellet}}\right) \times \left(\frac{\text{pellet}}{\text{sample area}}\right)$$

(34)

x = effective sample thickness

Therefore, by using (31), (34), and the incident power, the absorp-
tion coefficient may be caluclated from (30). In order to compare this
data with other methods, it is necessary to consider an approximate rela-
tionship with the imaginary part of the complex refractive index. This is
given by

$$\eta = k\lambda/4\pi$$

It is realized that there isn't any direct simple relationship between the absorption coefficient k and imaginary part η unless the real part of the complex refractive index matches that of the KBr host pellet at all experimental wavelengths. Therefore, the results of these experiments and calculations given in and compared to the other methods in Table I must be viewed with caution. Nonetheless, it should be noted that there is some reasonable agreement. Of course, the real part of the complex refractive index does vary drastically within the 9.2 micrometer wavelength region for quartz and therefore, application of the above approximate comparison is meaningless there.

As indicated above, the results of these experiments and calculations are given in Table I as approximate imaginary refractive index values for comparative purposes only. A system absorption sensitivity of 460 V/W on the 0.03 capacitance manometer scale was obtained by averaging the first two calibration methods. Data at other laser wavelengths than those listed in Table I are not readily available for comparison at this time.

As previously discussed, a major design criterion was to develop a spectrophone chamber with minimum response to scattered energy. One purpose of the 1.06 micrometer wavelength quartz test listed in Table I was to verify the ability of the spectrophone to separate effects due to scattering and absorption. It was expected that not much, if any, cell pressure signal would be observed, since quartz has a negligible absorption coefficient at this wavelength. However, scattering is known to occur. No signal was developed, implying little sensitivity to scattered energy.

Secondly, scattering sensitivity was tested by applying 15 to 25 micrometer diameter nonabsorbing glass spheres on the KBr pellet surface. A spectrophone signal of 0.96 volt was measured. Next an extinction test was taken as previously described. A 105 milliwatt loss was observed. This results in a scattering sensitivity of 9.1 V/W. Since the absorption sensitivity was about 460 V/W, the system ratio of absorption to scattering is greater than 50. Practical operation at shorter wavelengths is thus assured.

The system as delivered can make measurements at laser wavelengths from less than 0.5 micrometers to within the submillimeter range if

Table I

Absorption Index of Atmospheric Dust,
Quartz, and Soot

Particulate Matter	$\lambda(\mu m)$	Spectrophone[a] η	Other Method[b] η
Atmospheric	1.06	0.036	<0.023 [23,24]
dust	9.6	0.290	0.286 [25]
(assumed ρ =	10.6	0.135	0.145 [25]
2.4)			
Quartz	1.06	Negligible	$<10^{-07}$ [22]
(ρ = 2.66)	9.6	0.325	0.283 [22]
	10.6	0.051	0.034 [22]
Soot	1.06	0.586	0.65 [26]
(assumed ρ =	9.6	0.733	0.90 [26]
1.7)	10.6	0.732	

[a]Mean value of tests

[b]Interpolated data

-34-

proper windows and pellet host materials are used. As stated above, experimental tests have shown that the absorption to scattering sensitivity ratio is greater than 50 to 1. However, the experimental test that was used to determine this ratio only results in a lower bound. Actually, the scattering signal that did develop could have been mainly due to extra absorption from increased pathlengths through the host KBr pellet. Therefore, the 50 to 1 ratio could be very conservative. Almost all system tests were accomplished with less than 40 micrograms of sample per pellet, thereby requiring smaller time efforts in sample collection. The system turn-around time between different sample tests can be as low as 2-5 minutes. This should be more than adequate for multiple sample testing.

SYSTEM DISCRIPTION

The experimental basis and purpose of the system is to measure the absorption of laser light at a particular wavelength to measure the concentration of the absorbing gas.

Figure 13 shows the system layout. The experimental apparatus includes a spherical spectrophone (resonant cavity), laser, spectrum analyzer, power meter, audio signal generator, acoustic shield, bandpass filter/amplifier, microcomputer data acquisition subsystem, gas lines, and assorted optics.
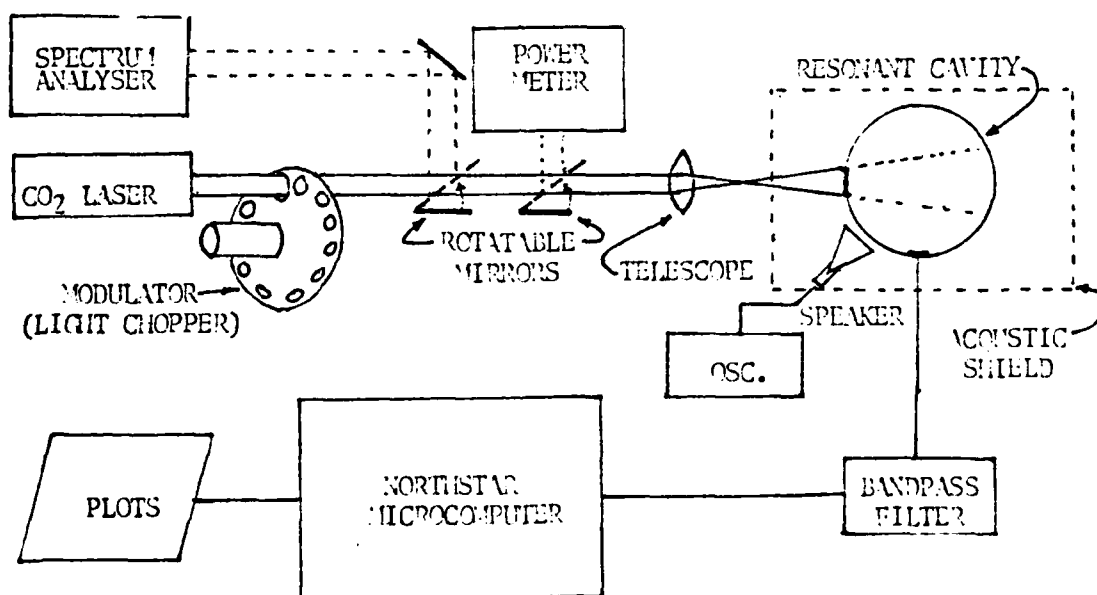
Figure 13. System Set-up

The laser source used is a CW CO_2 laser operating in the infrared portion of the electromagnetic spectrum at the 10P(20) line (10.6 micrometers) with an average power of 0.5 watts after the light chopper. The modulated beam is directed at the resonant cavity and its radiation absorbed by the test gas. Since the sphere has only one aperture all of the energy from the beam is introduced and subsequently reflected off the walls of the sphere.

The modulator (Ithaco light chopper with adjustable speed control) chops the infrared radiation at a frequency equivalent to the lowest order acoustic resonance of the resonant cavity. Radiation out of the chopper is approximately half of the incident laser power.

The first rotatable mirror after the chopper is used to reflect the CO_2 beam to a spectrum analyzer (Optical Engineering Inc. CO_2 Spectrum Analyzer). The second rotatable mirror is used for measuring the laser power to be introduced into the spectrophone. The beam is deflected onto a Scientech 362002 thermopile detector.

When the rotatable mirrors are out of the beam path, the CO_2 beam passes through a telescope which expands the beam causing a large beam spot at the back of the sphere for optimum dispersion of the electro-magnetic energy within the spectrophone. Care must be taken so that the beam out of the telescope can pass through the aperture of the acoustic shield and the NAC1 window.

The resonant cavity is shielded from spurious environmental noise _ by an acoustic shield as shown in Figure 14. It is constructed of 3-inch rock wool applied on 1/2 inch particle board in which the resonant cavity is mounted. The particle board reflects a large part of the acoustic energy directed at the sphere. Although most of the energy is reflected away, some sound will penetrate the wall. This energy is absorbed through the rock wool. In addition, the rock wool prevents any standing wave to occur inside the box by the energy that penetrated the rock wool. This is done by absorbing acoustic energy every time sound waves hit the rock wool. In this way, the acoustic energy is eventually nulled. However, in the experiment, not all the ambient sound was eliminated. This was due in a large part to the aperture in the shield. Another possibility is the transfer of energy from the bottom of the shield by the optical bench on which it was placed. The optical bench was caused to vibrate very slightly and this energy could have transferred to the sheield.
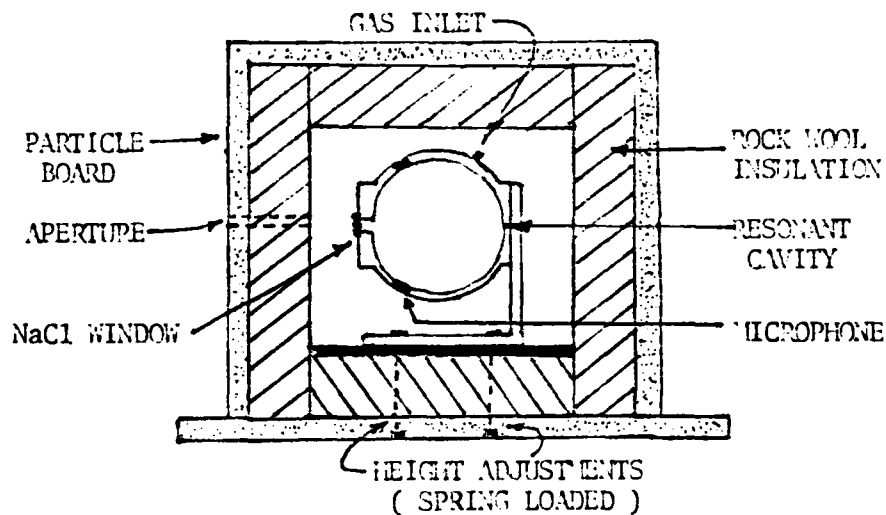
Figure 14. Cut-away View of the Acoustic Shield and Spectrophone

Spring loaded recessed bolts on the bottom of the shield mount onto the resonator stand with nuts. The tightness of the nuts finely adjusts the height of the sphere for proper introduction of the CO_2 chopped beam into the sphere. Not shown in the figure are the electrical and gas lines going out of the shield. THese lines are carefully recessed into the board for maximum insulation of the resonant sphere. Also not shown is an audio speaker used to excite the sphere at its resonance for band-pass filter adjustments.

The sphere is made of two machined hemispheres. The inside diameter is 6 inches. Electret microphones are mounted on the sphere so that the active side is flush to the inside wall. The aperture is centered on one of the flat ends of the sphere and sealed off with a NACl window. This particular window as selected because of its transparentness in the 10.6 micrometer region of the electromagnetic spectrum as shown in Figure 15.

The gas mixture to be studied is introduced through copper and flexible tubing to the gas inlet at the top of the resonant sphere.

The output of the electret microphones is filtered by an integrated UAF31 adjustable bandpass filter with a 100 Hz bandwidth and amplified by an inverting amplifier using a LM741 op-amp. The bandpass filter is used to eliminate very high and low frequency noise. The total gain is set at 8800.
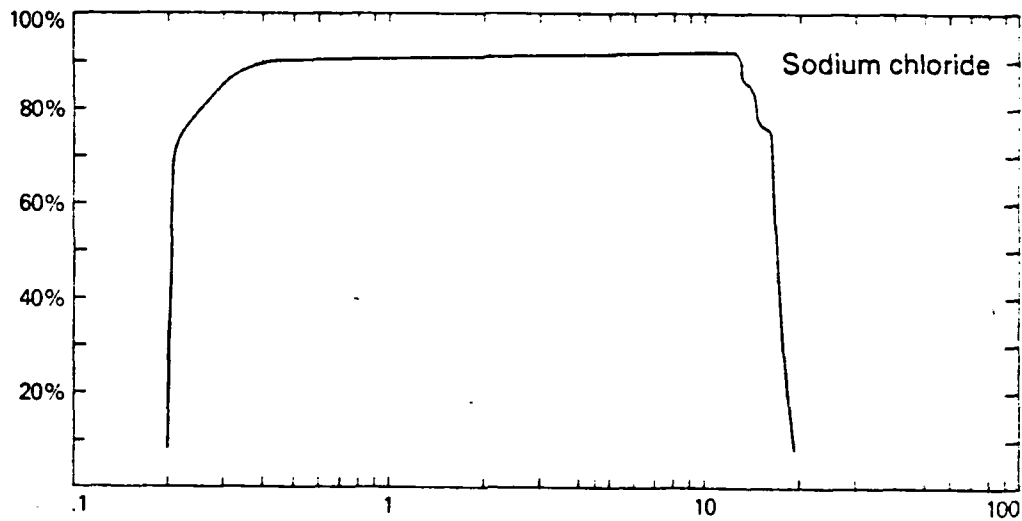
Figure 15. NACl Transmissibility Plot
Refractive index is 1.5 @ 10 μm
Source: 1979 Laser Focus Buyers' Guide

This roughly filtered signal is then processed by a Northstar Horizon II microcomputer system.   A more detailed description of the data acquisition system follows.

DATA ACQUISITION SYSTEM

The data acquisition and analysis system is designed to obtain data from the spectrophone, perform detailed calculations and analysis of the data, and provide a hardcopy of th results. The Organizational Flowchart, Figure 16, shows the organization for the main part of the data acquisition and analysis system.
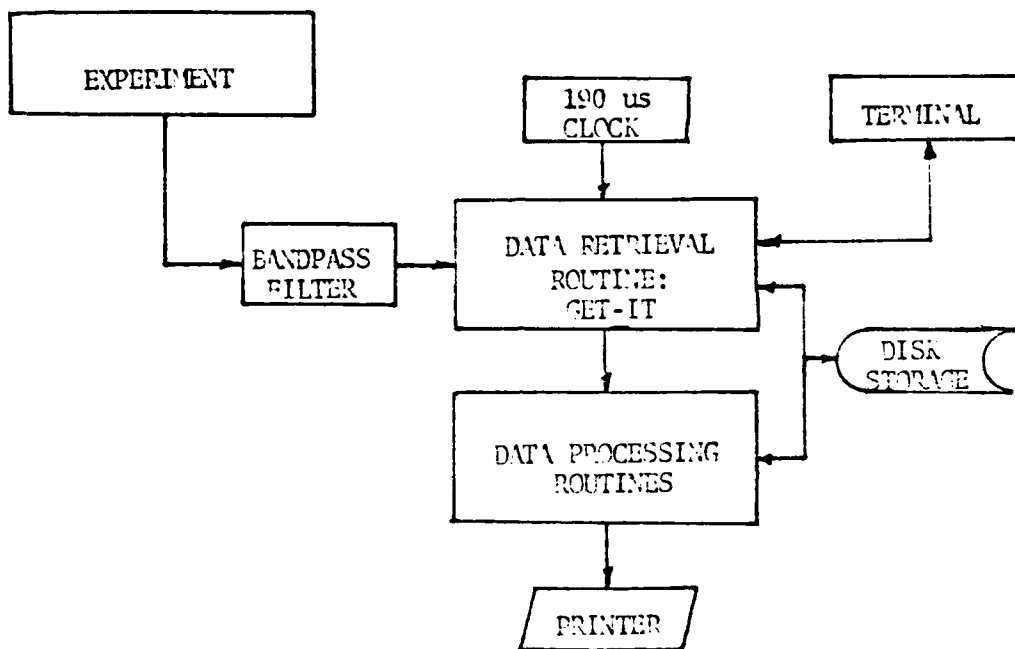

Figure 16. Organizational Flowchart for the Experiment

The Northstar Horizon II is a microcomputer with 54K of RAM and an extra disk drive. It is used in an interactive way with the operator to take and analyze data from the spectrophone. It provides the experimenter with a hard copy of the plots and a diskette with the results.

The Horizon II is capable of taking data from the spectrophone using a Cromemco 7-channel analog input/output board. The computer communicates with the operator via a CRT terminal. The hard copy is provided by a DECwriter III.

The microcomputer performs the following programs in sequence to arrive at a plot of the results:

1. GET-IT

GET-IT is the first program in the series. It asks the operator for the lower and upper frequency limits to be printed on the plots, the signal multiplication factors, and whether a hard copy is desired. This information is stored in file "FACTOR.DAT" on a diskette. The data is then taken with an assembly language subroutine SUX which takes exactly 4096 data points every 190 microseconds. This raw data is stored in file "ARRAY1.DAT" for the lower 2048 elements, and "ARRAY2.DAT" for the upper 2048 elements. This data is then processed by a Tukey window in subroutine TUKEY and this data is in turn bit-reversed by subroutine BITREV and restored in files "ARRAY1.DAT: and "ARRAY2.DAT". The bit-reversed data is then processed by EKFTR to obtain the real part of the FFT; the results are stored in "REAL1.DAT" and "REAL2.DAT" for the lower and upper elements respectively. Figures 17, 18, 19, and 20 are flow-charts of the program GET-IT and its subroutines. For a discussion of the bit-reversal process, see Appendix A and see Appendix B for FFT methods.

2. EKFFTI

This program uses the Radix-2 FFT method because of insufficient memory. An imaginary number array is created and filled with zeroes. Real data is retrieved from "REAL1.DAT" and an FFT is performed for the imaginary part. The result is stored in file "IMAG1.DAT". Sub- _ routine RADIX2 is then called and the upper part of the 4096 elements is processed and stored in "IMAG2.DAT". These two results are then combined in subroutine IMFFT which performs the final butterfly and placed the results in "IMAG1.DAT" and "IMAG2.DAT".

The routines LOPHAS and HIPHAS convert the real and imaginary compo-nents of the results of the lower and upper 2048 elements into phaser form. The flowchart for the Radix-2 operation is similar to Figure 20 with the substitution of the sine for the cosine function. The phaser routines are not flowcharted because they are simple calculations.

3. HZSTUF

HZSTUF takes the data in file "FACTOR.DAT" and determines the lower and upper analog frequency limits and stores the magnitude and phase
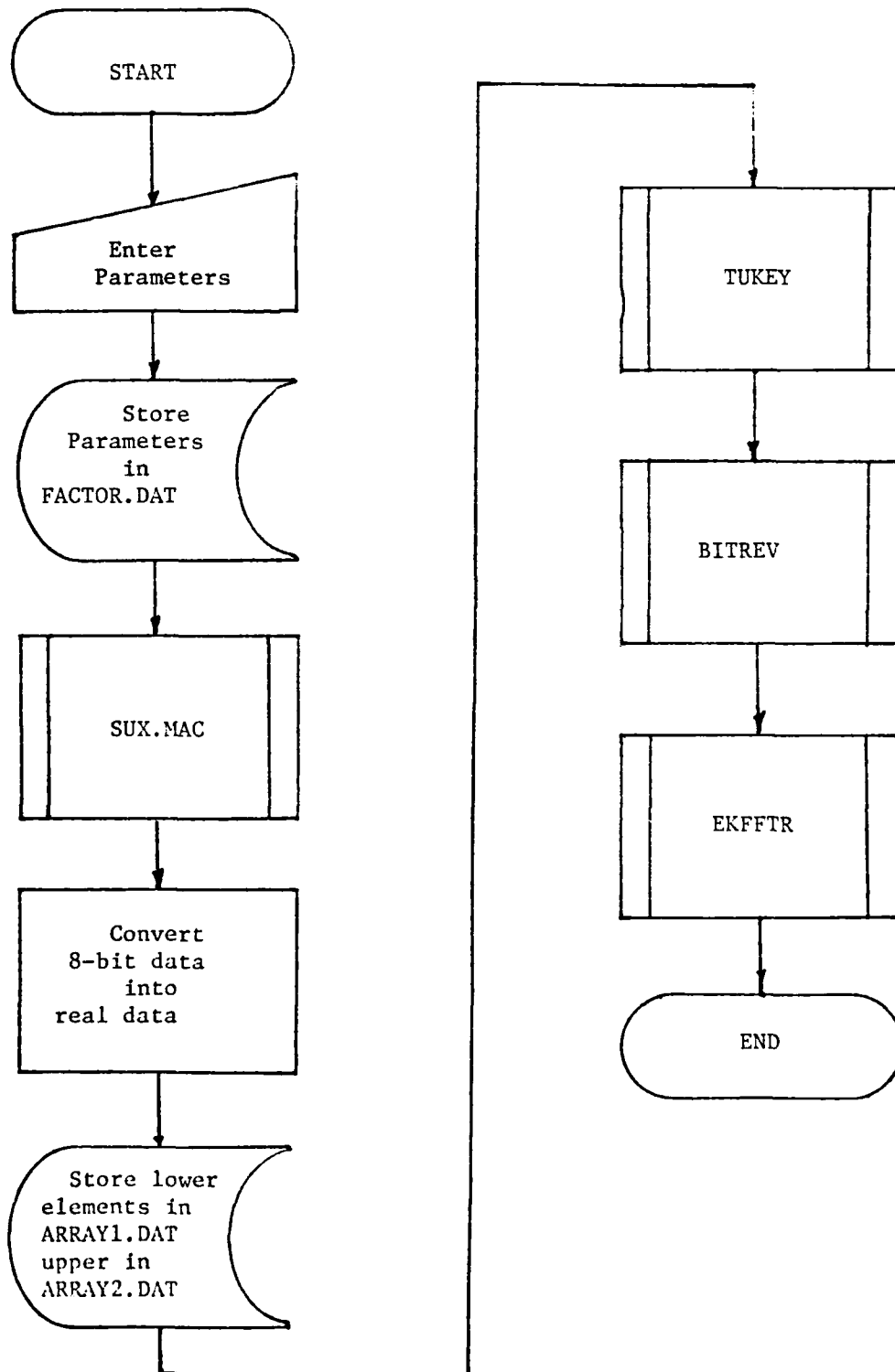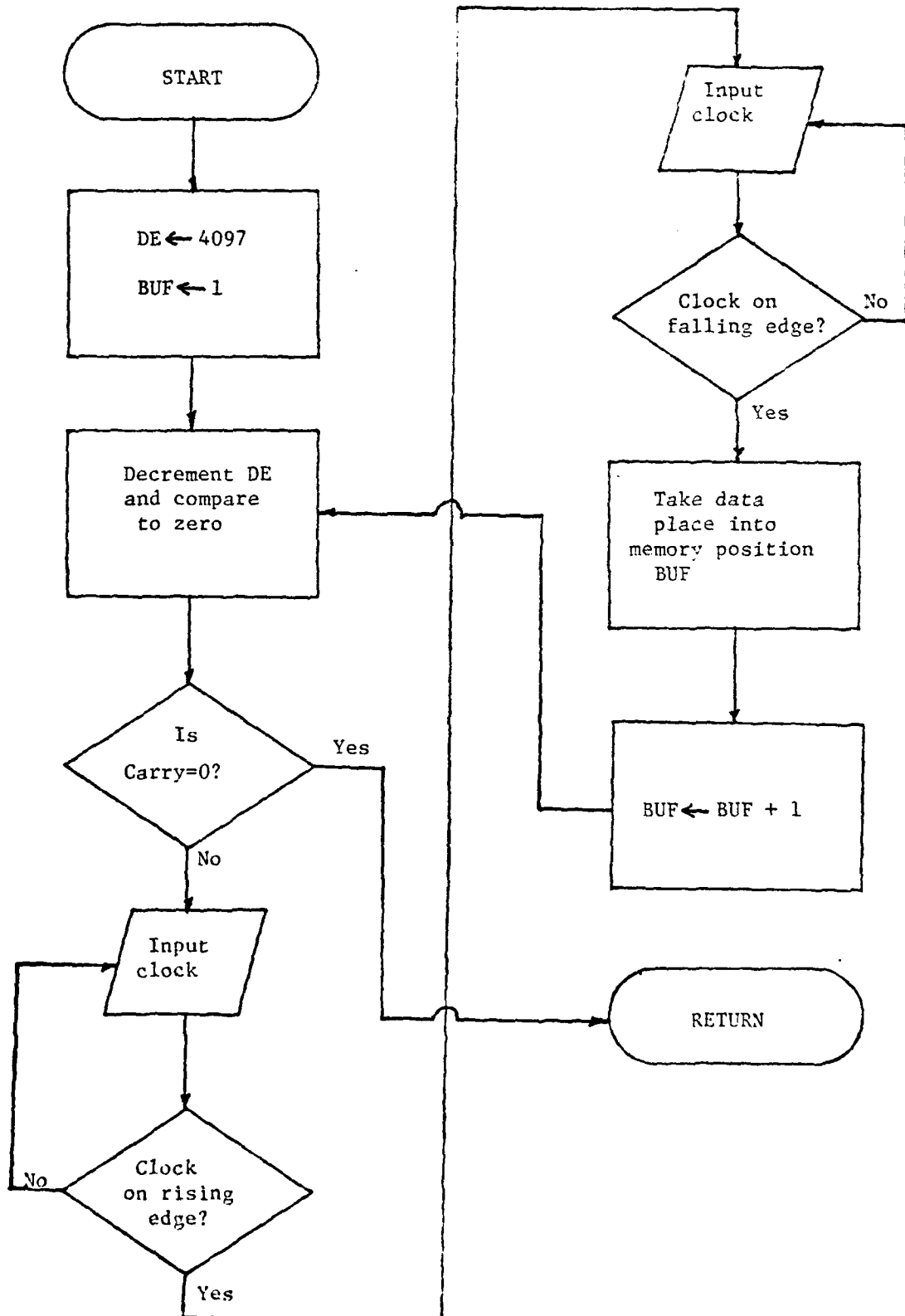
Figure 17.   Flowchart of GET-IT

-42-

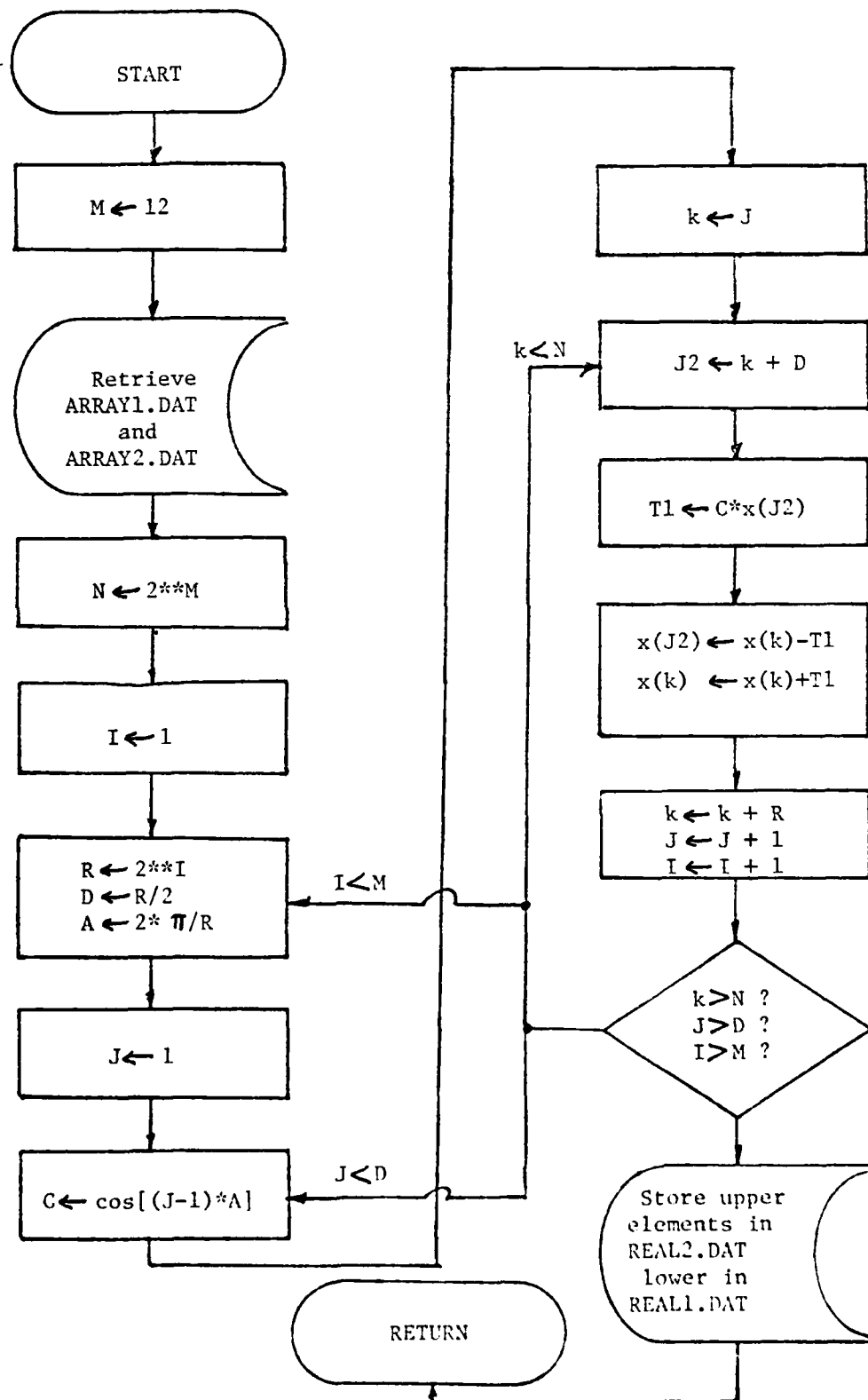Figure 18. Flowchart of SUX.MAC

Figure 19. Flowchart of EKFFTR

-44-
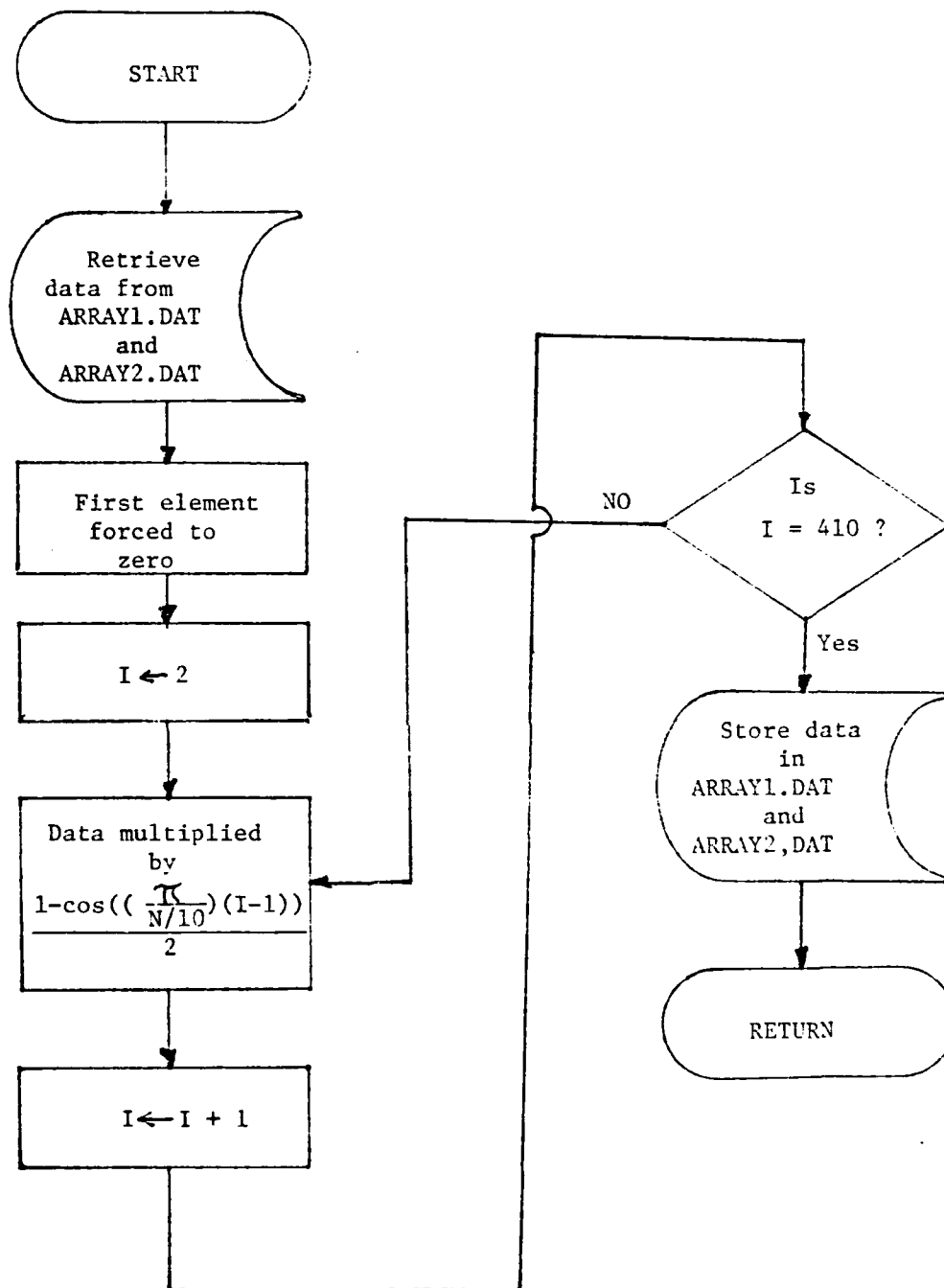
Figure 20. Flowchart of TUKEY

values in files "EMAG.DAT" and "DPHASE.DAT". The upper and lower frequency limits and spacing between the frequencies are stored in "HSDIV.DAT".

4. FREMAGPH

FREMAGPH determines the actual frequency values for the phasers. These values are stored in file "FREQ.DAT". The phasers with their corresponding magnitude and phase data read from files "EMAG.DAT" and "DPHASE.DAT" are printed.

5. PLOT

PLOT provides a graph of the results.

EXPERIMENTAL PROCEDURE

Before an experiment can be performed, residual gases in the sphere must be removed. In order to do this, the spectrophone must be pumped out to near vacuum and flushed several times with N_2. After several N_2 evacuations, introduction of a specific amount of test gas in N_2 may be made. In this experiment, the host gas in N_2 and the gas to be analyzed is CO_2. The mixture is held at atmospheric pressure, or 660 torr.

Upon introduction of the mixture, the audio speaker is turned on and the acoustic resonance of the sphere is found. The bandpass filter is then connected into the system and is tuned such that the center frequency of the filter corresponds to the acoustic resonant frequency f_a. The speaker is then turned off. The bandpass filter must be adjusted after every data aquisition since the resonance changes with temperature and pressure.

The laser is then turned on and the chopper adjusted to the resonant frequency of the sphere. Prior to actually introducing the laser beam into the spectrophone, the wavelength and power of the radiation is adjusted so that the laser is at the 10P (20) line and 0.5 W average power is into the sphere.

The beam is then directed into the spectrophone and the chopper speed is again adjusted to give maximum signal out of the spectrophone. The chopper frequency is defined to be f_c and the observed signal frequency is defined to be f_s. The program sequence is then started with the operator introducing relevant information to the computer and activating the 190 microsecond clock. The operator introduced information consists of a hardcopy request, the lower frequency of interest, the higher frequency of interest and the gain. Parameters normally entered are a lower frequency of 2300 Hz, a higher frequency of 2500 Hz, and a gain of 1. The activation of the clock starts the data conversion from analog to digital by sampling data every 190 microseconds. The A/D conversion is accomplished by an A/D board in the computer. A justification of the 190 microsecond sampling rate will follow.

After approximately 1 second, the data will have been taken and the data processing begins; culminating sometime later with a plot of voltage versus frequency.

Due to the narrowness of the spectrophone signal, as shown in Figure 21, the chopper must be held as steady as possible for the 1 second that the data will be taken.
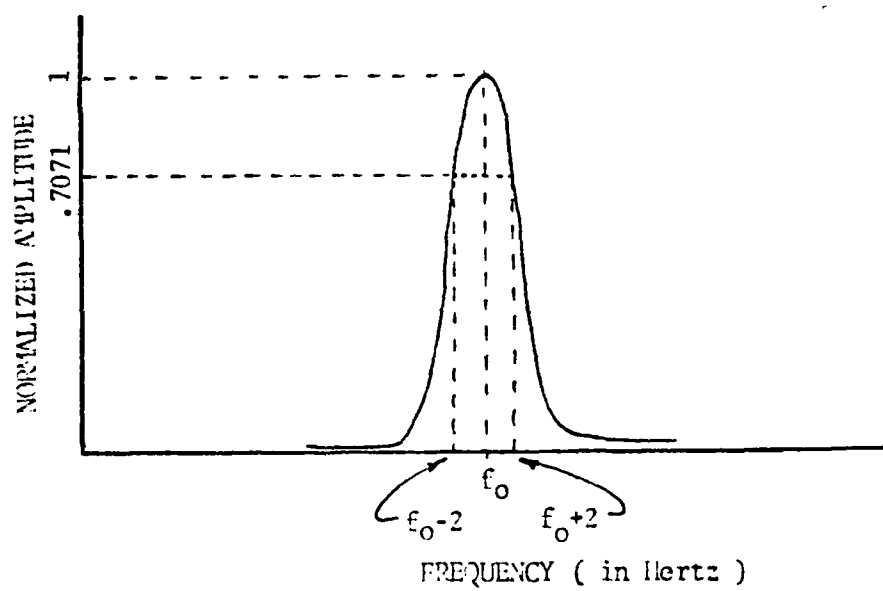
Figure 21. Acoustic Gain at Resonance

DATA ANALYSIS METHODS

Infrared absorption produces excited vibrational-rotational states
in the absorbing molecules, and visible and ultraviolet radiation produces
excited electronic levels [4]. Collisions between the excited molecules
and the background gas increase the translational energy (and hence the
pressure) of the sample. A microphone connected to the wall of the
chamber is used to detect this increase in pressure. The acoustic signal
is proportional to the intensity of the incoming radiation and to the
concentration of the absorbing species. Intense optical sources will
therefore allow the detection of smaller concentrations of absorbing gas.
In addition, multipassing the beam through the gas will also increase the
sensitivity of the chamber.

The two laser attributes of particular advantage to optoacoustic
systems are monochromaticity and high power. The fact that lasers are
highly monchromatic means that the potential exists for matching strong
gas absorption lines with suitable laser sources to achieve specificity.
Only molecules with absorption at the laser wavelength will participate
in producing an acoustic signal.

The high power available from laser sources makes possible increases
in the signal to be detected. When used wiht high quality microphones,
laser excited spectrophones have a wide dynamic range of gas concentrations.
The dynamic range available is limited by certain background signals
which are themselves proportional to laser power. These background sig-_
nals include window and wall effects which cause considerable problems
in data interpretation.

An additional advantage of a spectrophone system operating at reso-
nance is the enhancement of the acoustic signal. Assuming that the reso-
nance of the spectrophone is 2400 Hz, from Figure 21, the acoustic Q will
be approximately 600. The high Q available from a spherical system was
a major factor in using that geometry.

There are certain stipulations on the efficiency of the spectro-
phone however. The most notable being that the reciprocal of the vibra-
tional relaxation time τ be small compared to the resonant $\omega(s)$. That is,

$$\omega\tau \gg 1.$$

This criteria was met in this particular experiment.

Due to the high Q of the spherical system, the phase-sensitive lock-in amplifier could not be used to gather data due to its long time constants and varying resonance of the sphere. The instability of the chopper and possibly minute fluctuations in temperature disabled the responsiveness of the lock-in amplifier. Therefore, a microcomputer was used to gather and perform a FFT on the data.

The highest frequency of modulation was limited at 2600 Hz by the chopper; therefore, that frequency was used as the highest frequency of operation. In order to meet the Nyquist criteria, the sampling rate was to be at least two times the maximum frequency which in this case was 5200 Hz or 190 microseconds.

The number of data points that could be taken was limited by the size of the microcomputer memory. The largest number of data points that could be taken which was a power of two was 2^{12} or 4096 points. Since each number is represented by 4 bytes by the computer, the data occupied 16384 bytes of memory. This in addition to the memory occupied by the compiler and the programs came very close to the 54 K of RAM available in the microcomputer.

The data taken was then processed by the microcomputer using the Cooley-Tukey FFT algorithm and the results in the frequencies of interest were printed.

TEST RESULTS

The acoustic resonant frequency may be found by solving wave equations which yield solutions containing Bessel functions. However, since the resonant frequency changes with temperature and pressure, a solution arrived at by this method is both tedious and of little value. An alternative method of finding the resonance without tedious mathematics is worthwhile since it would yield a ballpark figure for the resonant frequency. Such a solution assumes an infinitely thin cylinder through the center of the sphere. The cylinder will therefore have a length equal to the inside diameter (d) of the sphere. The first mode will be a single period sinusoid with a null in the center. The frequency of the first resonance will be

$$\frac{c}{d} = f_a$$

where c is the speed of sound, 3.31×10^2 meters/second. The sphere in this experiment was 0.1397 meters in diameter. Therefore, the calculated resonant frequency was 2369 Hz. In order to obtain the exact frequency of resonance, the audio oscillator was varied about 2369 Hz until a peak signal was detected by the microphone.

What actually happens inside a sphere has not been investigated. An understanding of the resonant characteristics of a sphere could be extremely valuable. However, the lack of literature on this subject prevents a better understanding of the acoustic characteristics of the sphere.

The graph obtained from the host gas, N_2, is shown in Figure 22. The audio resonance, f_a, was 2420 Hz, the chopper frequency, f_c, was 2424 Hz, and the signal frequency, f_s, was 2457 Hz. Note that there are two sharp peaks, one at 2420 Hz and the other at 2460 Hz. It appears that the smaller peak represents the chopper noise and the larger peak the signal induced by wall and window effects of the N_2.

Compare the N_2 plot with that obtained by introducing 5: 655 torr CO_2 mixture in Figure 23. Again f_a = 2420 Hz, f_c = 2424 Hz, and f_s = 2457 Hz. Note however, that the larger peak is now 51 mV compared to 31 mV of the N_2 effects. This result definitely shows a presence of CO_2 although a difference in signals could not be determined by casual
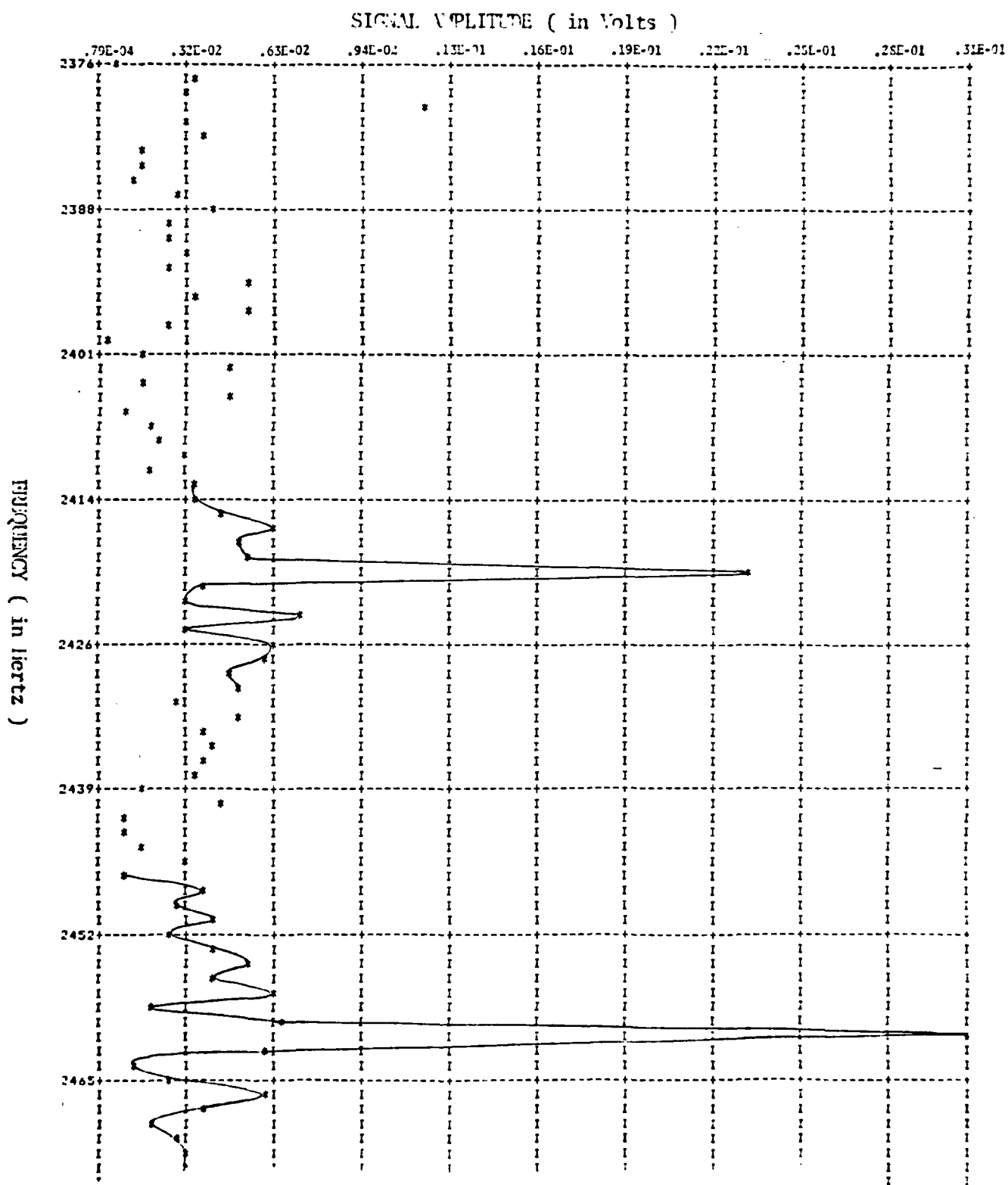
SIGNAL AMPLITUDE (in Volts)

Figure 22. Plot of N_2 at 660 torr. Large signal due
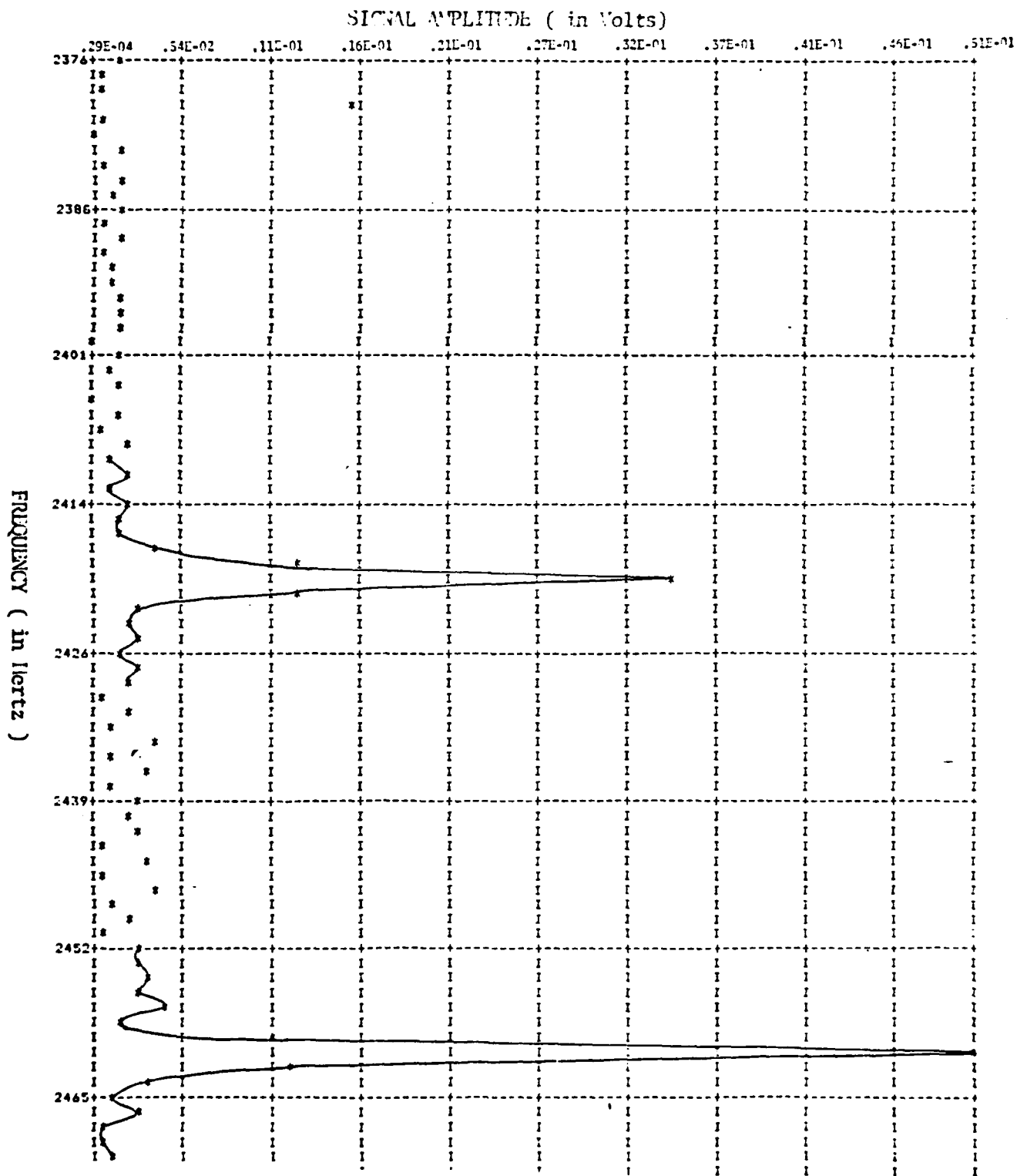to wall and window heating effects.

Figure 23. Plot of 5 : 655 torr CO_2 mixture. Note that
the signal is a full 20 mV higher than the N_2 signal.

observation of the signals on an oscilloscope due to random noise burying the actual signal. The comparison of methods just mentioned conclusively demonstrates the superiority of the signal processing method to oscilloscope observations. And if the smaller peak is the chopper noise, the FFT method is better than the lock-in amplifier technique because of its resolution. Shown in Figure 24 is a plot of N_2 data over the one second interval in which the data was taken. This graph clearly shows erratic and fast fluctuations of the signal caused by either the chopper instability or resonance fluctuations. Such fluctuations were intolerable to the phase-sensitive lock-in amplifier which was used during one phase of the experiment. The constant fluctuation caused phase mismatch between the spectrophone signal and the reference signal causing unreliable measurements. Again, by carefully controlling the chopper for just one second, the signal processing method appears better than the lock-in amplifier technique.

Nitrogen was used as a host gas because it does not absorb energy at 10.6 micrometers. Carbon dioxide was used because of its availability. However Table 1 shows the CO_2 is not a good absorber at 10.6 micrometers. This indicates that the microcomputer-spherical spectrophone is a moderately sensitive device.
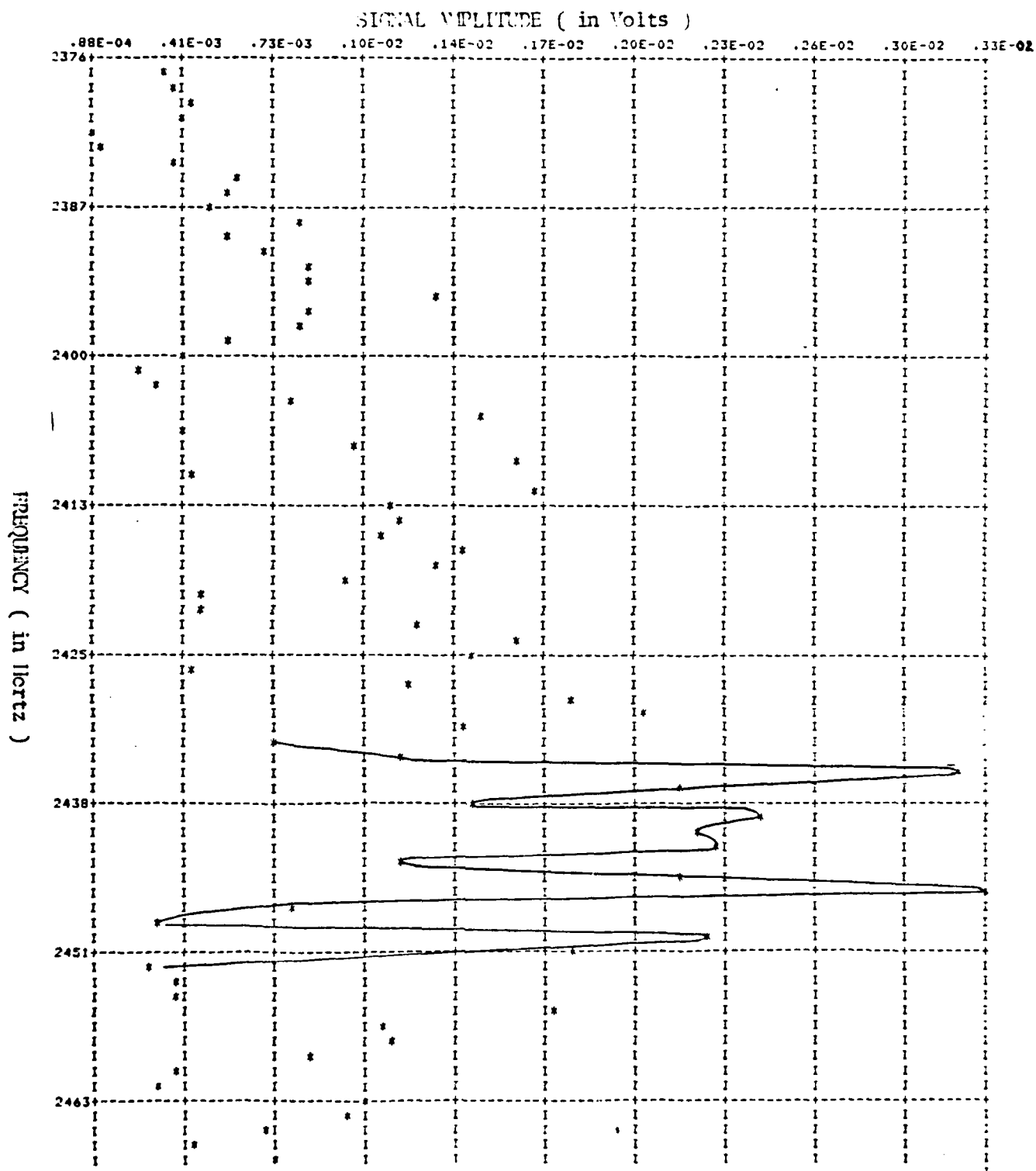
Figure 24. Signal Fluctuation due to Unstable Chopper

Gas	Sensitivity [atm-cm]	Laser Line	Absorption coefficient [atm-cm]$^{-1}$	Wavelength [μm]
Nitric oxide	10^{-2}	$^{12}C^{16}O$:7-6,P(15)	3.5	5.19
Sulfur dioxide	10^{-2}	$^{12}C^{18}O_2$:00°1-II,R(40)	0.55	9.02
Ozone	2×10^{-4}	$^{12}C^{18}O_2$:00°1-II,P(40)	14	9.50
	2×10^{-4}	$^{12}C^{16}O_2$:00°1-II,P(14)	13	9.50
Ethylene	5×10^{-5}	$^{12}C^{16}O_2$:00°1-I,P(14)	30	10.53
Ammonia	10^{-4}	$^{12}C^{16}O_2$:00°1-I,P(32)	17	10.72
Carbon Dioxide	2×10^{-1}	$^{12}C^{16}O_2$:00°1-I,P(20)	0.015	10.59

Table II. Measured sensitivities of fixed-frequency laser lines to pollutant gases. The gases were at 298 K, except NO which was at 390 K, and CO_2, which was at 450 K. The background gases were either N_2 or O_2. The band designations I and II refer to the upper and lower of the mixed CO_2 ($10^{0}0$, $02^{0}0$) states, respectively.

Source: Hindley, E.D., Topics in Applied Physics, 14, Springer-Verlag, New York, 1976, p. 325.

CONCLUSIONS

PELLET SPECTROPHONE

The design and construction of the herein described pellet spectrophone has illustrated that a differential system can be constructed to measure low level absorption by atmospheric dust. Furthermore, it has been shown that an absorption to scattering sensitivity greater than 50 can be achieved, which is a necessary property for measuring absorption at short wavelengths. Thus, pellet spectrophones permit measurements at visible and infrared wavelengths to be directly compared.

Detection capability of microwatts of absorbed energy is possible with this system. Therefore, milliwatt sources and microgram samples may be utilized. The small amount of sample needed is important when using materials which are hard to collect.

Since the absorption and scattering coefficients are not independent, surrounding the dust with a material (KBr) having a refractive index different than air can cause errors in the absorption measurement. The size distribution of the particulate sample within the KBr host material can also be important, especially in wavelength regions where strong absorption and resultant shadowing can occur. However, if all of these problems are recognized, the pellet spectrophone system does result in good measurements of the absorption coefficients of the suspended material at whatever wavelengths tested and at whatever size distributions that exist in the host KBr pellet. It does not result in any data directly convertible to complex refractive index determination except, perhaps under special conditions. The best potential use of the pellet spectrophone might occur in the submillimeter wavelength region where the difference in sample particle size and those sizes in air might not be important due to the larger wavelengths resulting in minimal scattering losses. Here, the measured absorption might be directly converted to the imaginary part of the complex refractive index. This application is being investigated and will be reported on in the future.

SPHERICAL SPECTROPHONE

This system proved to be very difficult to use because of its high Q characteristics. Small fluctuatons in the resonance or the chopper caused large signal variations. Although the system gain was high, the spectrophone was not as sensitive as hoped for. Wall and window effects amplified with the actual absorption signal caused undesireable results.

The system did, however, prove to be extremely interesting and was moderately sensitive. The data acquisition system proved invaluable in a resonant spherical spectrophone system and may prove equally vital in other systems. Calibration of the system would have to be done with the wall effects since these signals dominate.

Future studies could investigate the relationship that the wall signal has to the phase difference between it and the input modulation and the absorption signal. Phase analysis could prove vital in understanding the sperical spectrophone and may be used to better isolate the absorption signal.

Due to the difficulty of testing suspended aerosol media, all of the above testing used gas mixtures. Aerosol testing will be resumed when and if more sensitivity is obtained.

REFERENCES

1. Schleusener, S. A., J. D. Lindberg, K. O. White, and R. L. Johnson, "Spectrophone Measurements of Infrared Laser Energy Absorption by Atmospheric Dust", Applied Optics 15, 2546 (1976).

2. Hass, M., et al., "Measurement of Very Low Absorption Coefficients by Laser Calorimetry", Applied Optics 14, 1128 (1975).

3. Jones, M. W. and K. E. Kao, "Spectrophotometric Studies of Ultra Low Loss Optical Glasses II: Double Beam Method", Journal of Scientific Instruments 2, 331 (1969).

4. Stierwalt, D. L., "Infrared Spectral Emittance Measurements of Optical Materials", Applied Optics 5, 1911 (1966).

5. Lindberg, J. D. and L. S. Laude, "Measurement of the Absorption Coefficient of Atmospheric Dust", Applied Optics 13, 1923 (1974).

6. Rosencwaig, A., "Photoacoustic Spectroscopy of Solids", Physics Today, 23 (September 1975).

7. Hordvik, A. and H. Schlossberg, "Photoacoustic Technique for Determining Optical Absorption Coefficients in Solids", Applied Optics 16, 101 (1977).

8. Bell, A. G., "Production of Sound by Light", Bulletin of the Philosophical Society of Washington, 4, 161 (April 1881).

9. Kruezer, L. B., "Ultralow Gas Concentration Infrared Absorption Spectroscopy", Journal of Applied Physics, 42, 7 (June 1971).

10. Dewey, C. F., et al., "Acoustic Amplifier for Detection of Atmospheric Pollutants", Applied Physics Letters 23, 633 (December 1973).

11. Rosengren, L., "A New Theoretical Model of the Opto-Acoustic Gas Concentration Detector", Infrared Physics 13, 109 (1976).

12. Bennett, H. S. and R. A. Forman, "Absorption Coefficients in Highly Transparent Solids: Barothermal Theory for Cylindrical Configurations", Applied Optics 14, 3031 (1975).

13. Bennett, H. S. and R. A. Forman, "Absorptions Coefficients of Weakly Absorbing Solids: Theory of a Barothermal Gas Cell", Applied Optics 15, 347 (1976).

14. Bennett, H. S. and R. A. Forman, "Photoacoustic Methods for Measuring Surface and Bulk Absorption Coefficients in Highly Transparent Materials: Theory of a Gas Cell", Applied Optics 15, 2405 (1976).

15. Deaton, T. F., D. A. Depatie, and T. W. Walker, "Absorption Coefficient Measurements of Nitrous Oxide and Methane at DF Laser Wavelengths", Applied Physics Letters 26, 300 (1975).

16. Born, M. and E. Wolf, <u>Principles of Optics</u>, Pergamon Press, Oxford (1975) pp. 55-70.

17. Macdonald, J., <u>Metal-Dielectric Multilayers</u>, Elsevier, New York (1971).

18. Weinstein, W., "Computations in Thin Film Optics", Vacuum, $\underline{4}$, 3 (January 1954).

19. Peterson, J. T. and J. A. Weinman, "Optical Properties of Quartz Dust Particles at Infrared Wavelengths", J. Geophysical Research $\underline{74}$, 6947 (1969).

APPENDIX A

BIT-REVERSAL

The bit-reversal process is a method of separating the odd

and even array elements. In addition, the use of this process

expedites the Cooley-Tukey FFT algorithm. An eight element array

is bit-reversed below as an example:

x(0) → x(000)		x(000) → x(0)
x(1) → x(001)		x(100) → x(4)
x(2) → x(010)		x(010) → x(2)
x(3) → x(011)	$\Longrightarrow$	x(110) → x(6)
x(4) → x(100)		x(001) → x(1)
x(5) → x(101)	Bit-	x(101) → x(5)
x(6) → x(110)	Reversal	x(011) → x(3)
x(7) → x(111)		x(111) → x(7)

Note that the first 4 elements are now even and the rest

are odd.

APPENDIX B

FAST FOURIER TRANSFORMS

The FFT is an algorithm that decomposes DFT computations
into successively smaller DFT computations. The particular
algorithm used in this experiment is a decimation-in-time algorithm.
That is, data in the time domain is converted to the frequency
domain.

The decimation-in-time algorithm is most conveniently illustrated
by letting the number of samples N be a power of 2; i.e.,

$$N = 2^m$$

Since N is an even integer, $X(k)$ may be computed by separating $x(n)$
into two $N/2$ sequences, one even and the other odd. Knowing that
$X(k)$ is given by

$$X(k) = \sum_{n=0}^{N-1} x(n)W_N^{nk} \quad , k=0, 1, 2, \ldots, N-1$$

where

$$W_N^{nk} = e^{-j(2\pi/N)kn}$$

and separating the odd and even $x(n)$, we obtain

$$X(k) = \sum_{n \text{ even}} x(n)W_N^{nk} + \sum_{n \text{ odd}} x(n)W_N^{nk}$$

Letting $n = 2r$ for n even and $n = 2r + 1$ for n odd,

$$X(k) = \sum_{r=0}^{(N/2)-1} x(2r)W_{N/2}^{rk} + W_N^k \sum_{r=0}^{(N/2)-1} x(2r + 1)W_{N/2}^{rk}$$

$$= G(k) + W_N^k H(k)$$

A flow graph of the above is given in Figure 25.

The Tukey window is used prior to the bit-reversal routine.

Windowing is used to suppress the side lobes, thus creating
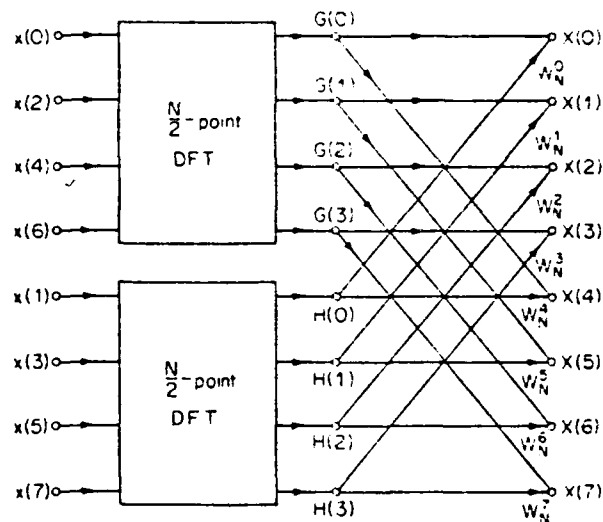
better resolution.

Figure 25.   Flow graph of the decimation-in-time decomposition
             of an N-point DFT computation into two N/2 DFT
             computations (N=8).

   Source: Oppenheim, A.V., Schafer, R.W., _Digital Signal_
             Processing, Prentice Hall, New Jersey, 1975, p. 291.